Kroenke, L. W., Berger, W. H., Janecek, T. R., et al., 1991
Proceedings of the Ocean Drilling Program, Initial Reports, Vol. 130

2. EXPLANATORY NOTES[1]

Shipboard Scientific Party[2]

INTRODUCTION

In this chapter, we have assembled information regarding the recovery of materials, the presentation of results, and the conventions used to identify samples. This information concerns only shipboard operations and analyses described in the site reports in the *Initial Reports* volume of the Leg 130 *Proceedings of the Ocean Drilling Program*. The methods used by various investigators for shore-based analysis of Leg 130 data will be detailed in the individual scientific contributions published in the *Scientific Results* volume.

AUTHORSHIP OF SITE CHAPTERS

The separate sections of the site chapters were written by the following shipboard scientists (authors are listed in alphabetical order in parentheses; no seniority is implied). Authors who participated in the editing of this volume at the first Leg 130 postcruise meeting are denoted with an asterisk.

Site Summary (Berger*, Kroenke*)
Background and Objectives (Berger, Kroenke)
Operations (Janecek*, Pollard)
Sedimentology and Lithostratigraphy (Janecek, Jansen, Krissek*, Lind, Mosher, Prentice, Schmidt, Wu)
Biostratigraphy (Backman, Corfield, Lange, Leckie*, Resig, Takahashi, Takayama)
Paleomagnetics (Musgrave, Tarduno)
Sediment Accumulation Rates (Backman)
Inorganic Geochemistry (Delaney)
Carbon Geochemistry (Stax)
Igneous Petrology (Mahoney, Storey)
Physical Properties (Bassinot, Marsters, Mayer, Wilkens)
Downhole Measurements (Lyle*, Mayer, Wilkens)
Seismic Stratigraphy (Mayer*)
Summary and Conclusions (Berger, Kroenke)
Appendix (Shipboard Scientific Party)

Following the text of each site chapter are summary core descriptions ("barrel sheets" and igneous rock visual core descriptions) and photographs of each core.

SURVEY AND DRILLING DATA

Use of "Ma" vs "m.y."

The abbreviation "Ma" is equivalent to and replaces m.y. B.P. (million years before present); for example, 35–40 Ma. The abbreviation "m.y." is used in such sentences as "... for 4 m.y. in the early Miocene" to denote a number of years rather than a specific point in time.

Drilling Characteristics

Information concerning sedimentary stratification in uncored or unrecovered intervals may be inferred from seismic data and wireline-logging results as well as from an examination of the behavior of the drill string as observed and recorded on the drilling platform. Typically, the harder a layer, the slower and more difficult it is to penetrate. A number of other factors may determine the rate of penetration, so it is not always possible to relate the drilling time directly to the hardness of the layers. Bit weight and revolutions per minute, recorded on the drilling recorder, also influence the penetration rate.

Drilling Deformation

When cores are split, many show signs of significant sediment disturbance, including the concave-downward appearance of originally horizontal bands, haphazard mixing of lumps of different sediment types (mainly at the tops of cores), and the near-fluid state of some sediments recovered from tens to hundreds of meters below the seafloor. Core deformation probably occurs during cutting, retrieval (with accompanying changes in pressure and temperature), and core handling on deck. A detailed discussion of slumplike drilling disturbance is given in the "Core Description" section of this chapter.

SHIPBOARD SCIENTIFIC PROCEDURES

Numbering of Sites, Holes, Cores, and Samples

Ocean Drilling Program (ODP) drill sites are numbered consecutively. A site consists of one or more holes drilled while the ship was positioned over one acoustic beacon. Multiple holes may be drilled at a single site by pulling the drill pipe above the seafloor (out of the hole), moving the ship some distance from the previous hole, and then drilling another hole.

For all ODP drill sites, a letter suffix distinguishes each hole drilled at the same site. The first hole drilled is assigned the site number modified by the suffix A, the second hole has suffix B, and so forth. Note that this procedure differs slightly from that used by Deep Sea Drilling Project (DSDP) Sites 1 through 624 in which the first hole has no suffix. Adding a suffix for each hole prevents ambiguity between site- and hole-number designations. It is important to distinguish among holes drilled at a site, because recovered sediments or rocks from different holes usually do not have equivalent depths for equivalent stratigraphic positions.

The cored interval is measured in meters below seafloor (mbsf). The depth interval assigned to an individual core begins with the depth below the seafloor that the coring operation began and extends to the depth that the coring operation ended (see Fig. 1). For example, each coring interval is generally up to 9.5 m long, which is the length of a core barrel. Coring intervals may be shorter than that. Also, cores are not adjacent if separated by drilled intervals. In soft sediments, the drill string can be "washed ahead" with the core barrel in place, without recovering sediments. This is achieved by pumping water down the pipe at high pressure to wash the sediment out of the way of the bit and up the space between the drill pipe and the wall of the

[1] Kroenke, L. W., Berger, W. H., Janecek, T. R., et al., 1991. *Proc. ODP, Init. Repts.*, 130: College Station, TX (Ocean Drilling Program).
[2] Shipboard Scientific Party is as given in the list of participants preceding the contents.

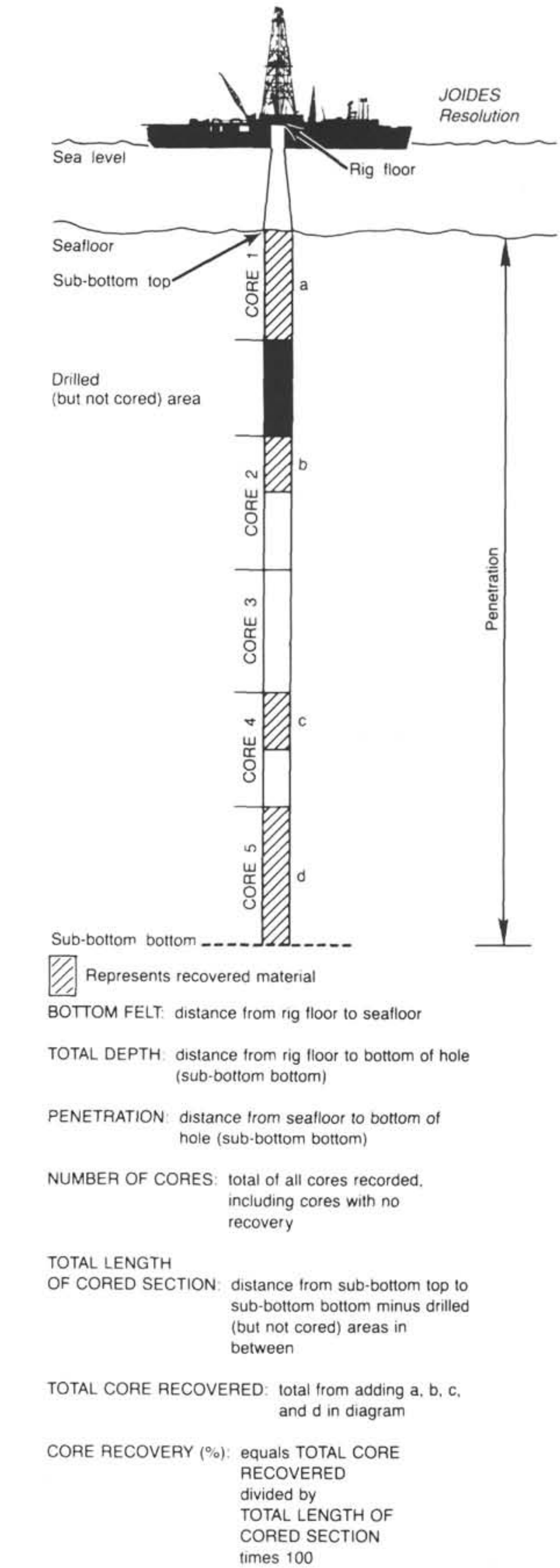

Figure 1. Coring and depth intervals.

hole. If thin, hard, rock layers are present, then it is possible to get "spotty" sampling of these resistant layers within the washed interval and thus have a cored interval greater than 9.5 m. In drilling hard rock, a center bit may replace the core barrel if it is necessary to drill without core recovery.

Cores taken from a hole are numbered serially from the top of the hole downward. Core numbers and their associated cored intervals in mbsf usually are unique in a given hole; however, this may not be true if an interval must be cored twice because of the caving of cuttings or other hole problems. The maximum full recovery for a single core is 9.5 m of rock or sediment contained in a plastic liner (6.6-cm internal diameter) plus about 0.2 m (without a plastic liner) in the core catcher (Fig. 2). The core catcher is a device at the bottom of the core barrel that prevents the core from sliding out when the barrel is being retrieved from the hole. In certain situations (e.g., when coring gas-charged sediments that expand while being brought on deck), recovery may exceed the 9.5-m maximum.

A recovered core is divided into 1.5-m sections that are numbered serially from the top (Fig. 2). When full recovery is obtained, the sections are numbered from 1 through 7, with the last section possibly being shorter than 1.5 m (rarely, an unusually long core may require more than 7 sections). When less than full recovery is obtained, there will be as many sections as needed to accommodate the length of the core recovered (e.g., 4 m of core would be divided into two 1.5-m sections and one 1-m section). If cores are fragmented (recovery <100%), sections are numbered serially and intervening sections are noted as void, whether shipboard scientists believe that the fragments were contiguous *in situ* or not. In rare cases, a section <1.5 m may be cut to preserve features of interest (e.g., lithologic contacts).

By convention, material recovered from the core catcher is placed below the last section when the core is described and labeled core catcher (CC); in sedimentary cores, it is treated as a

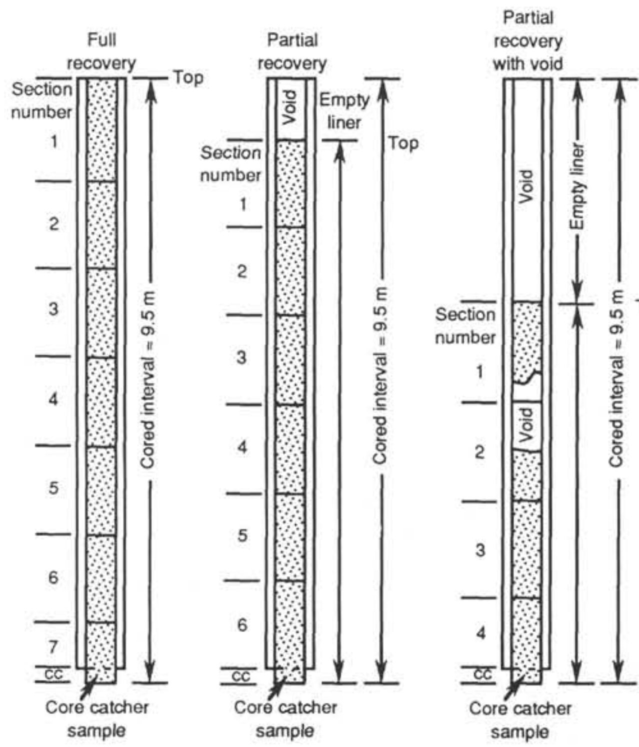

Figure 2. Examples of numbered core sections.

separate section. The core catcher is placed at the top of the cored interval in cases where material is only recovered in the core catcher. However, information supplied by the drillers or by other sources may allow for more precise interpretation as to the correct position of core-catcher material within an incompletely recovered cored interval.

Igneous rock cores are also cut into 1.5-m sections that are numbered serially; each piece of rock is then assigned a number. Fragments of a single piece are assigned a single number, and individual fragments are identified alphabetically. The core-catcher sample is placed at the bottom of the last section and is treated as part of the last section, rather than separately. Scientists completing visual core descriptions describe each lithologic unit, noting core and section boundaries only as physical reference points.

When the recovered core is shorter than the cored interval, the top of the core is equated with the top of the cored interval by convention to achieve consistency in handling analytical data derived from the cores. Samples removed from the cores are designated by distance measured in centimeters from the top of the section to the top and bottom of each sample removed from that section. In curated hard rock sections, sturdy plastic spacers are placed between pieces that did not fit together to protect them from damage in transit and in storage; therefore, the centimeter interval noted for a hard rock sample has no direct relationship to that sample's depth within the cored interval, but is only a physical reference to the location of the sample within the curated core.

A full identification number for a sample consists of the following information: leg, site, hole, core number, core type, section number, piece number (for hard rock), and interval in centimeters measured from the top of section. For example, a sample identification of "130-803A-25R-1, 10–12 cm" would be interpreted as representing a sample removed from the interval between 10 and 12 cm below the top of Section 1 in Core 25 (R designates that this core was taken during rotary drilling) of Hole 803A during Leg 130.

All ODP core and sample identifiers indicate core type, using the following abbreviations: H = advanced hydraulic piston corer (APC); R = rotary core barrel (RCB); P = pressure core barrel; X = extended core barrel (XCB); B = drill-bit recovery; C = center-bit recovery; I = *in-situ* water sample; S = sidewall sample; W = wash-core recovery; and M = miscellaneous material. APC, XCB, RCB, and W cores were cut on Leg 130.

Core Handling

Sediments

As soon as a core was retrieved on deck, a sample was taken from the core catcher and given to the paleontological laboratory for an initial age assessment. The core was then placed on a long horizontal rack, and gas samples were taken by piercing the core liner and withdrawing gas into a vacuum tube. Voids within the core were sought as sites for gas sampling. Some of the gas samples were stored for shore-based study, but others were analyzed immediately as part of the shipboard safety and pollution-prevention program. Next, the core was marked into section lengths, each section was labeled, and the core was cut into sections. Interstitial water (IW), organic geochemistry (OG), and whole-round physical properties (PP) samples were also taken at this time. In addition, some headspace gas samples were scraped from the ends of cut sections on the catwalk and sealed in glass vials for light hydrocarbon analysis. Afterward, each section was sealed at the top and bottom by gluing on color-coded plastic caps: blue to identify the top of a section and clear for the bottom. A yellow cap was placed on the section ends from which a whole-round sample was removed. The caps were usually attached to the liner by coating the end liner and the inside rim of the cap with acetone and then attaching the caps to the liners.

The cores then were carried into the laboratory, where the sections were labeled with an engraver to mark the full designation of the section permanently. The length of the core in each section and the core-catcher sample were measured to the nearest centimeter; this information was logged into the shipboard CORELOG data-base program.

Whole-round sections from APC and XCB cores were normally run through the multisensor track (MST). The MST includes the gamma-ray attenuation porosity evaluator (GRAPE), the *P*-wave logger, and a volume magnetic susceptibility meter. After the core had equilibrated to room temperature (approximately 3 hr), thermal conductivity measurements were performed on fairly soft sediments, and the cores were split.

Cores of soft material were split lengthwise into working and archive halves. The softer cores were split with a wire or saw, depending on the degree of induration. Harder cores were split with a band saw or diamond saw. The wire-cut cores were split from the bottom to top, so investigators should be aware that older material could have been transported up the core on the split face of each section.

The working half of the core was sampled for shipboard and shore-based laboratory studies. Each sample extracted was logged into the sampling data-base program by the location and the name of the investigator receiving the sample. Records of all of the samples removed are kept by the curator at ODP headquarters. The extracted samples were sealed in plastic vials or bags and labeled. Samples were routinely taken for shipboard physical property analysis. These samples were subsequently used for calcium carbonate (coulometric) and organic carbon (CNS elemental) analyses; these data are reported in the site chapters.

The archive half was then described visually. Smear slides were made from samples taken from the archive half and were supplemented by thin sections taken from the working half. Most archive sections were run through the cryogenic magnetometer. The archive half was photographed with both black-and-white and color film, a whole core at a time. Close-up photographs (black-and-white) were taken of particular features, as requested by individual scientists, for illustrations in the summary of each site.

Both halves of the core were put into labeled plastic tubes, which were then sealed and transferred to cold-storage space aboard the drilling vessel. At the end of the leg, the cores were transferred from the ship in refrigerated air-freight containers to cold storage at the Gulf Coast Repository of the Ocean Drilling Program, Texas A&M University, College Station, Texas.

Igneous and Metamorphic Rocks

Igneous and metamorphic rock cores were handled differently from sedimentary cores. Once on deck, the core-catcher was placed at the bottom of the core liner and total core recovery was calculated by shunting the rock pieces together and measuring to the nearest centimeter; this information was logged into the shipboard CORELOG data-base program. The core then was cut into 1.5-m-long sections and transferred into the laboratory.

The contents of each section were transferred into 1.5-m-long sections of split core liner, where the bottom of oriented pieces (i.e., pieces that clearly could not have rotated top to bottom about a horizontal axis in the liner) were marked with a red wax pencil to ensure that orientation was not lost during the splitting and labeling process. The core was then split into archive and working halves. A plastic spacer was used to separate individual pieces and/or reconstructed groups of pieces in the core liner. These spacers may represent a substantial interval of no recovery. Each piece was numbered sequentially from the top of each section, beginning with number 1; reconstructed groups of pieces were assigned the same number but were lettered consecutively. Pieces were labeled only on external surfaces. If the piece was oriented, an arrow was added to the label pointing to the top of the section.

The working half of the hard-rock core was sampled for shipboard laboratory studies. Records of all samples are kept by the curator at ODP headquarters. Minicore samples were taken routinely for physical properties and magnetic studies. Some of these samples were subdivided at a later time for X-ray fluorescence (XRF) analysis and thin-sectioning, so that as many measurements as possible were made on the same pieces of rock. At least one minicore was taken per lithologic unit when recovery permits, generally from the freshest areas of core. Additional thin sections, X-ray diffraction (XRD) samples, and XRF samples were selected from areas of particular interest. Samples for shore-based studies were selected in a sampling party held after drilling had ended.

The archive half was described visually, then photographed with both black-and-white and color film, one core at a time. Both halves of the core were then shrink-wrapped in plastic to prevent rock pieces from vibrating out of sequence during transit, put into labeled plastic tubes, sealed, and transferred to cold-storage space aboard the drilling vessel.

VISUAL CORE DESCRIPTION

Sediment "Barrel Sheets"

The core description forms (Fig. 3), or "barrel sheets," summarize the data obtained during shipboard analysis of each sediment core. The following discussion explains the ODP conventions used in compiling each part of the core description forms and the exceptions to these procedures adopted by the Leg 130 scientific party.

Shipboard sedimentologists were responsible for visual core logging, smear slide analyses, and thin-section descriptions of sedimentary and volcaniclastic material. Mineral composition data, determined by X-ray diffraction, were used to augment the visual core descriptions. Data on biostratigraphy (age), geochemistry ($CaCO_3$, C_{org}), paleomagnetics, and physical properties (wet-bulk density and porosity) were integrated with the sedimentological information.

Core Designation

Cores are designated using leg, site, hole, core number, and core type as discussed in the section on "Numbering of Sites, Holes, Cores, and Samples" (this chapter). The cored interval is specified in terms of meters below seafloor (mbsf). Based on drill-pipe measurements (dpm) reported by the SEDCO coring technician and the ODP operations superintendent, depths are corrected for the height of the rig floor dual elevator stool above sea level to give true water depth and correct depth in meters below sea level (mbsl).

Paleontological Data

Microfossil abundance, preservation, and zone assignment appear on the core description form under the heading "Biostrat. Zone/Fossil Character." The chronostratigraphic unit, as recognized on the basis of paleontological results, is shown in the "Time-Rock Unit" column. Detailed information on the zonations and terms used to report abundance and preservation is presented in the "Biostratigraphy" section (this chapter).

Paleomagnetic, Physical Properties, and Chemical Data

Columns are provided on the core description form for recording paleomagnetic results (normal, reversed, or unknown polarity, shown as "N," "R," or "?", respectively), physical properties values (wet-bulk density and porosity), and chemical data (percentages of $CaCO_3$ determined with the Coulometrics analyzer). Additional information on shipboard procedures for collecting these types of data appears in the "Paleomagnetism," "Physical Properties," and "Organic Geochemistry" sections (this chapter).

Graphic Lithology Column

The lithology of the material recovered is represented on the core description forms by a single symbol or by two or more symbols (see Fig. 4) in the column titled "Graphic Lithology." Where an interval of sediment or sedimentary rock is a homogeneous mixture, the constituent categories are separated by a solid vertical line, with each category represented by its own symbol. Constituents comprising $<25\%$ of the sediment are not put in the graphic lithology column but are listed in the "Lithologic Description" section of the barrel sheet. In an interval composed of two or more sediment types that have quite different composition, such as thin-bedded and highly variegated sediments, the average relative abundances of the constituents are represented graphically by dashed lines that vertically divide the interval into appropriate fractions, as described above.

The graphic lithology column only shows the composition of layers or intervals exceeding 10 cm in thickness. Information on finer scale lithologic variations is included in the visual core description (VCD) forms available from ODP upon request.

Where sedimentary material was intercalated with igneous rocks, the igneous petrologists described the igneous section and recorded the results in "Hard Rock Core Description Forms." These are referred to on the sedimentary barrel sheets as "igneous rock" or "basalt."

Sedimentary Structures

In sediment cores, natural structures and structures created by the coring process can be difficult to distinguish. Natural structures observed are indicated in the "Sedimentary Structure" column of the core description form. The symbols used to describe the primary biogenic and physical sedimentary structures, and secondary structures such as microfaults, dewatering veinlets, and mineral-filled fractures, are given in Figure 5. In describing sediments recovered during Leg 130, the use of two of these symbols was modified:

1. Throughout most of the recovered intervals, the symbol for "planar laminae" is used to indicate the presence of color bands. True planar laminae were observed only in the basal clastic sediments at Sites 803 and 807; in all cases, the meaning of this symbol is described in the barrel sheet text.
2. In deeper portions of the recovered intervals, the symbol for "Convoluted/Contorted Beds" is used to indicate the presence of stylolites. Each feature (true convoluted/contorted beds and stylolites) is also noted in the appropriate barrel sheet text, so that the meaning of the symbol on each barrel sheet can be clarified by consulting its text.

Sediment Disturbance

Sediment disturbance resulting from the coring process is illustrated in the "Drilling Disturbance" column on the core description form (using the symbols in Fig. 5). Blank regions indicate a lack of drilling disturbance. The degree of drilling disturbance is described for soft and firm sediments using the following categories:

1. Slightly deformed: bedding contacts are slightly bent.
2. Moderately deformed: bedding contacts have undergone extreme bowing.

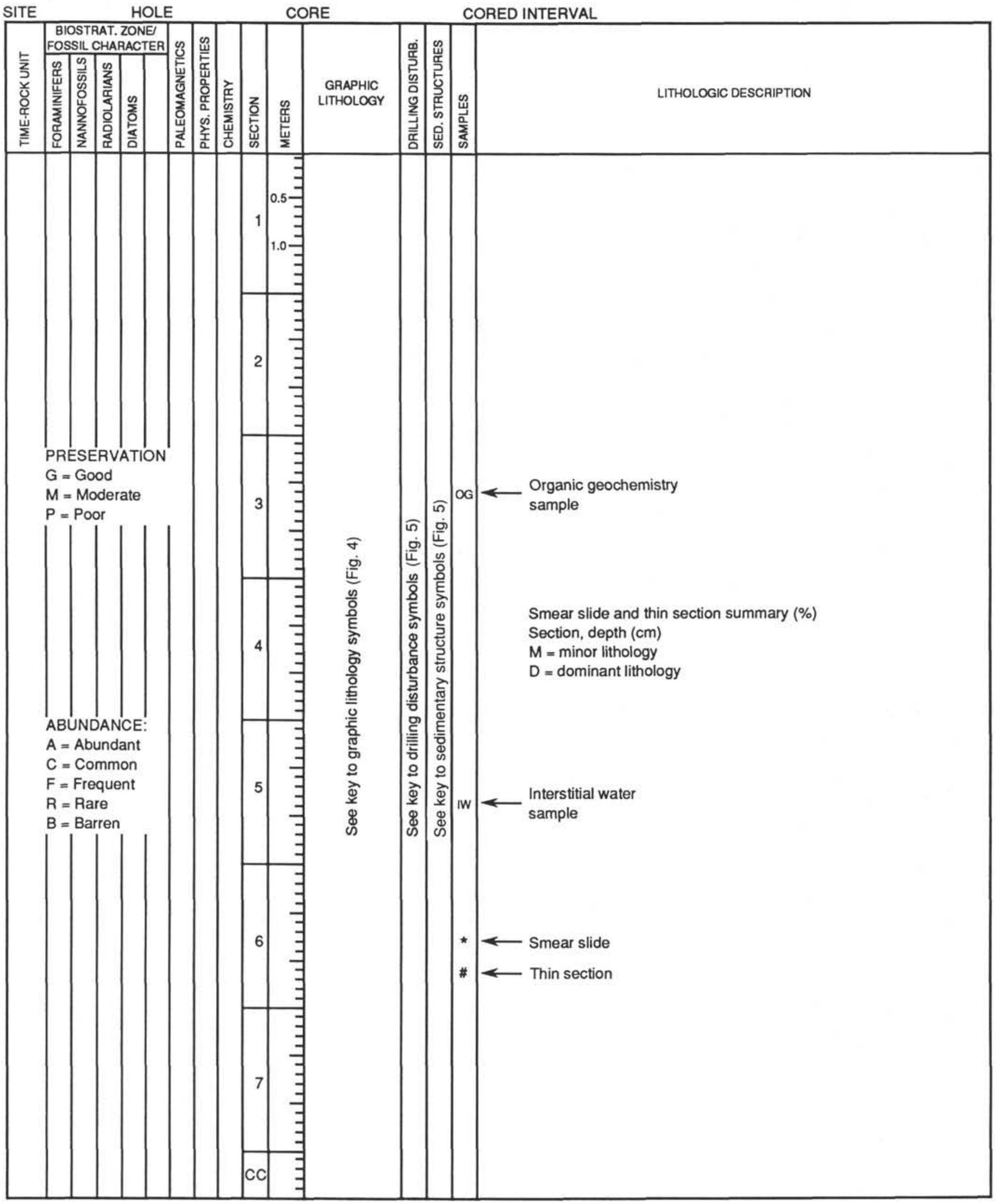

Figure 3. Core description form ("barrel sheet") used for sediments and sedimentary rocks.

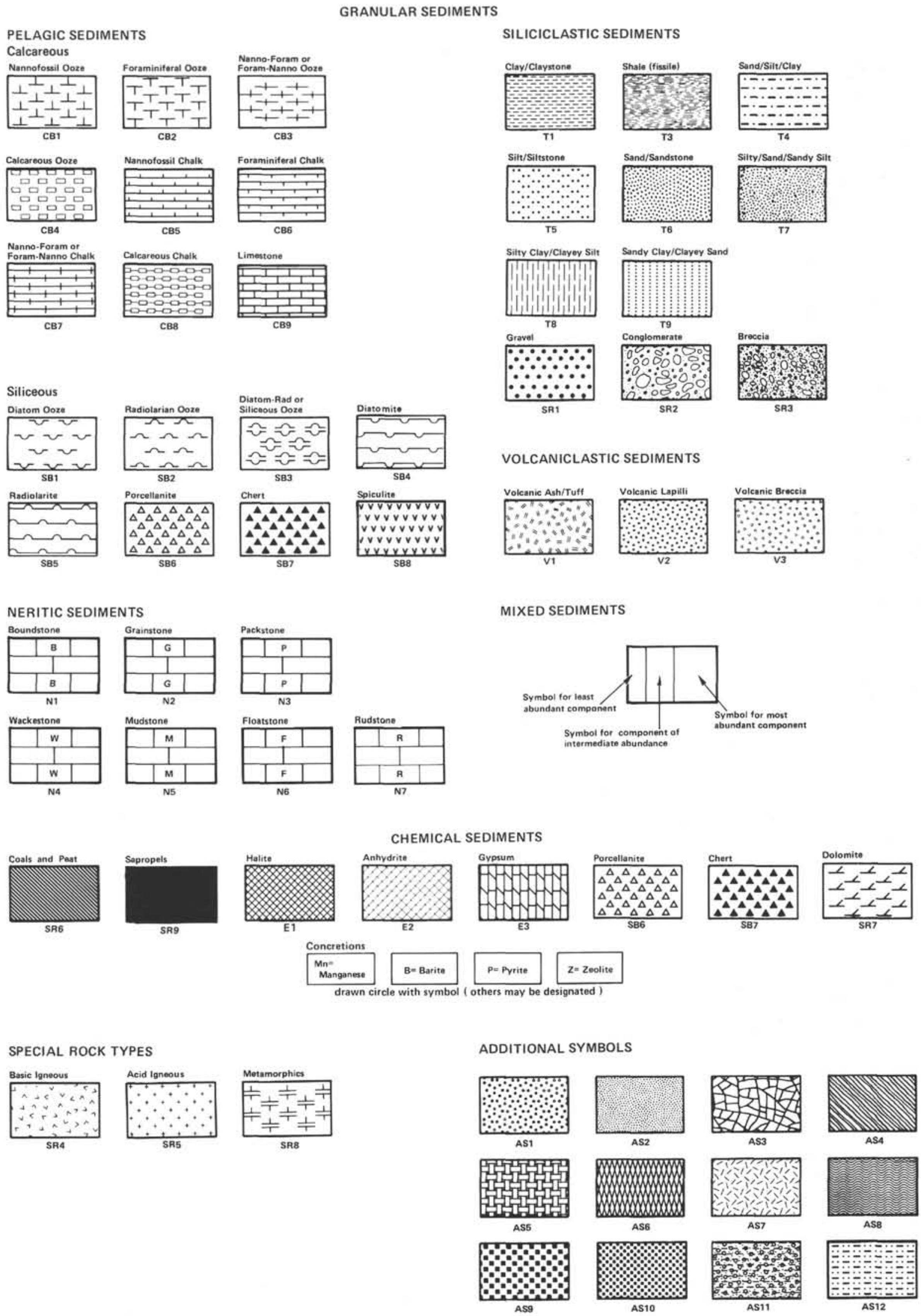

Figure 4. Key to symbols used in the "graphic lithology" column on the core description form shown in Figure 3.

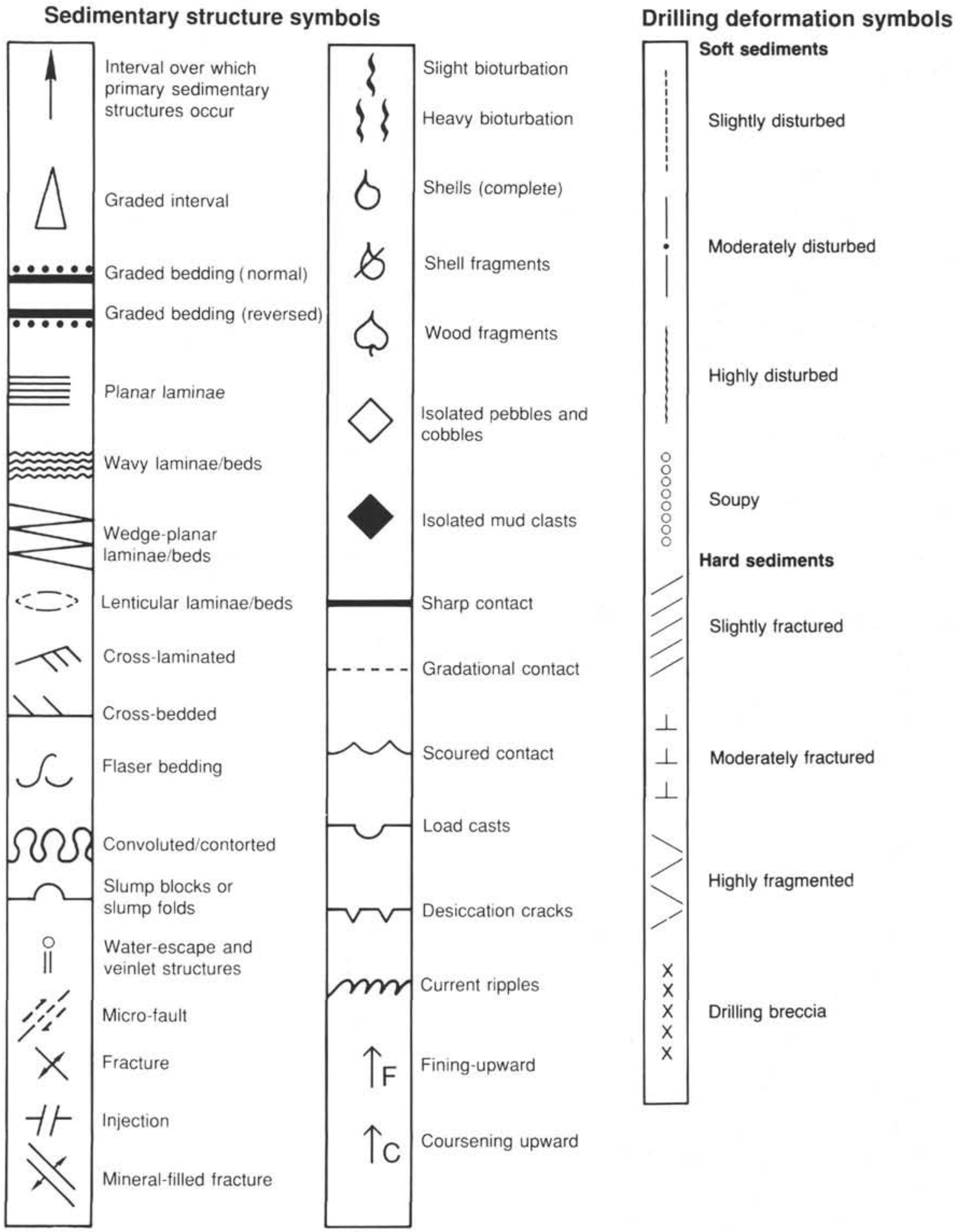

Figure 5. Key to symbols used for drilling disturbance and sedimentary structure on core description form shown in Figure 3.

3. Highly deformed: bedding is completely disturbed, sometimes showing symmetrical diapirlike or flow structures.

4. Soupy: intervals are water saturated and have lost all aspects of original bedding.

The degree of fracturing in indurated sediments and igneous rocks is described using the following categories:

1. Slightly fractured: core pieces are in place and contain little drilling slurry or breccia;

2. Moderately fragmented: core pieces are in place or partly displaced, but original orientation is preserved or recognizable (drilling slurry may surround fragments);

3. Highly fragmented: pieces are from the interval cored and probably in correct stratigraphic sequence (although they may not represent the entire section), but original orientation is completely lost;

4. Drilling breccia: core pieces have lost their original orientation and stratigraphic position and may be mixed with drilling slurry.

Induration

The criteria used to determine the induration of pelagic sediments found during Leg 130 are subjective and provide three classes for pelagic oozes:

1. Soft: sediments that have little strength and are readily deformed under the finger or broad blade of the spatula are termed oozes or clay;
2. Firm: partly lithified pelagic sediments such as oozes or clays that are readily deformed under the fingernail or the edge of a spatula blade;
3. Hard: nonfriable, cemented rocks.

The suffix "-stone" is added to the name of cemented rocks (e.g., limestone, claystone). Hard siliceous sedimentary rocks are called chert or porcellanite.

Color

Colors were determined by comparison with Munsell soil-color charts immediately after the cores were split because redox-associated color changes may occur when deep-sea sediments are exposed to the atmosphere. Information on core colors is given in the text of the "Lithologic Description" on the core description forms.

Samples

The position of samples taken from each core for shipboard analysis is indicated in the "Samples" column on the core description form (Fig. 3). The symbol "★" indicates the location of smear slide samples, and the symbol "#" indicates the location of thin-section samples. The notations IW and OG designate the location of samples for whole-round, interstitial-water geochemistry and frozen organic geochemistry, respectively.

Smear Slide Summary

A table summarizing data from smear slides and thin sections appears on each core barrel description form. The table includes information on the sample location, whether the sample represents a dominant ("D") or a minor ("M") lithology in the core, and the estimated percentages of sand, silt, and clay, together with all identified components. Note that smear slide analyses tend to underestimate the abundance of foraminifers and volcaniclastic-detrital material because these larger grains are difficult to incorporate into the smear.

Lithologic Description—Text

The lithologic description that appears on each core description form (barrel sheet) consists of two parts: (1) a heading that lists all the major sediment types (see "Sedimentology" section, this chapter) observed in the core; and (2) a more detailed description of these sediments, including data on color, location in the core, significant features, etc. Descriptions and locations of thin, interbedded, or minor lithologies are included in the text.

SEDIMENTOLOGY

The new sediment classification scheme for ODP by Mazzullo et al. (1988), partly reproduced below, was used during Leg 130. The sediment classification scheme described here defines two basic sediment types: (1) granular and (2) chemical.

Granular Sediments

Classes of Granular Sediments

Four types of grains are recognized in granular sediments: *pelagic, neritic, siliciclastic,* and *volcaniclastic* grains.

1. Pelagic grains are composed of the fine-grained skeletal debris of open-marine siliceous and calcareous microfauna and microflora (e.g., radiolarians, nannofossils) and associated organisms.
2. Neritic grains are composed of coarse-grained calcareous skeletal debris (e.g., bioclasts, peloids), and fine-grained calcareous grains of nonpelagic origin.
3. Siliciclastic grains are composed of mineral and rock fragments that were derived from plutonic, sedimentary, and metamorphic rocks.
4. Volcaniclastic grains are composed of rock fragments and minerals that were derived from volcanic sources.

Variations in the relative proportions of the four grain types define five major classes of granular sediments: *pelagic, neritic, siliciclastic, volcaniclastic,* and *mixed sediments* (Fig. 6).

1. Pelagic sediments are composed of >60% pelagic and neritic grains and <40% siliciclastic and volcaniclastic grains, and contain a higher proportion of pelagic than neritic grains.
2. Neritic sediments are composed of >60% pelagic and neritic grains and <40% siliciclastic and volcaniclastic grains, and contain a higher proportion of neritic than pelagic grains.
3. Siliciclastic sediments are composed of >60% siliciclastic and volcaniclastic grains and <40% pelagic and neritic grains, and contain a higher proportion of siliciclastic than volcaniclastic grains.
4. Volcaniclastic sediments are composed of >60% siliciclastic and volcaniclastic grains and <40% pelagic and neritic grains, and contain a higher proportion of volcaniclastic than siliciclastic grains. This class includes epiclastic sediments (volcanic detritus that is produced by erosion of volcanic rocks by wind, water, and ice), pyroclastic sediments (the products of the degassing of magmas), and hydroclastic sediments (the products of the granulation of volcanic glass by steam explosions).

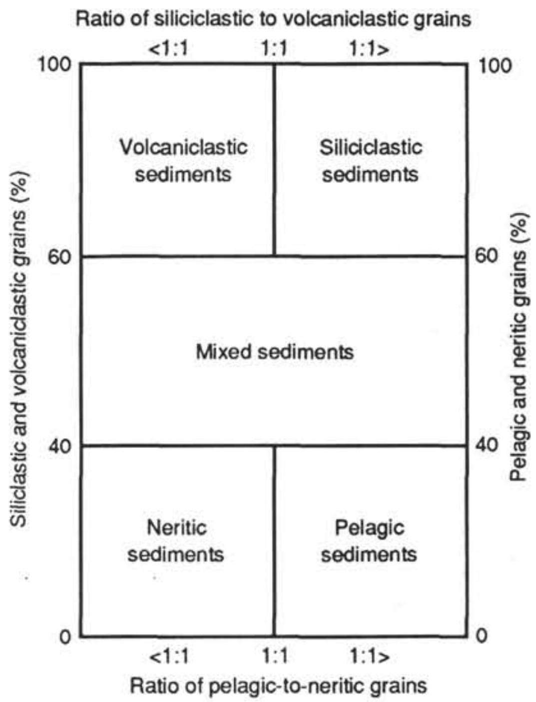

Figure 6. Diagram showing classes of granular sediment (modified from Mazzullo et al., 1988).

5. Mixed sediments are composed of 40%–60% siliciclastic and volcaniclastic grains, and 40%–60% pelagic and neritic grains.

Classification of Granular Sediment

A granular sediment can be classified by designating a *principal name* and *major* and *minor modifiers.* The principal name of a granular sediment defines its granular sediment class; the major and minor modifiers describe the texture, composition, fabric, and/or roundness of the grains themselves (Table 1).

Principal Names

Each granular sediment class has a unique set of principal names, which are outlined below.

For pelagic sediment, the principal name describes the composition and degree of consolidation using the following terms:

1. *Ooze:* unconsolidated calcareous and/or siliceous pelagic sediments.
2. *Chalk:* firm pelagic sediment composed predominantly of calcareous pelagic grains.
3. *Limestone:* hard pelagic sediment composed predominantly of calcareous pelagic grains.
4. *Radiolarite, diatomite,* and *spiculite:* firm pelagic sediment composed predominantly of siliceous radiolarians, diatoms, and sponge spicules, respectively.
5. *Porcellanite:* a well-indurated rock with abundant authigenic silica but less hard, lustrous, or brittle than chert (in part, such rocks may represent mixed sedimentary rock).
6. *Chert:* vitreous or lustrous, conchoidally fractured, highly indurated rock composed predominantly of authigenic silica.

For neritic sediment, the principal name describes the texture and fabric, using the following terms (from Dunham, 1962):

1. *Boundstone:* components organically bound during deposition.
2. *Grainstone:* grain-supported fabric, no mud, grains <2 mm in size.
3. *Packstone:* grain-supported fabric, with intergranular mud, grains <2 mm in size.
4. *Wackestone:* mud-supported fabric, with >10% grains, grains <2 mm in size.
5. *Mudstone:* mud-supported fabric, with <10% grains.
6. *Floatstone:* matrix-supported fabric, grains >2 mm in size.
7. *Rudstone:* grain-supported fabric, grains >2 mm in size.

Table 1. Outline of granular-sediment classification scheme (modified from Mazzullo et al., 1988).

Sediment class	Major modifiers	Principal names	Minor modifiers
Pelagic	1. Composition of pelagic and neritic grains present in major amounts 2. Texture of clastic grains present in major amounts	1. Ooze 2. Chalk 3. Limestone 4. Radiolarite 5. Diatomitie 6. Spiculite 7. Chert	1. Composition of pelagic and neritic grains present in minor amounts 2. Texture of clastic grains present in minor amounts
Neritic	1. Composition of neritic and pelagic grains present in major amounts 2. Texture of clastic grains present in major amounts	1. Boundstone 2. Grainstone 3. Packstone 4. Wackestone 5. Mudstone 6. Floatstone 7. Rudstone	1. Composition of neritic and pelagic grains present in minor amounts 2. Texture of clastic grains present in minor amounts
Siliciclastic	1. Composition of all grains present in major amounts 2. Grain fabric (gravels only) 3. Grain shape (optional) 4. Sediment color (optional)	1. Gravel 2. Sand 3. Silt 4. Clay (etc.)	1. Composition of all grains present in minor amounts 2. Texture and composition of siliciclastic grains present as matrix (for coarse-grained clastic sediments)
Volcaniclastic	1. Composition of all volcaniclasts present in major amounts 2. Composition of all pelagic and neritic grains present in major amounts 3. Texture of siliciclastic grains present in major amounts	1. Breccia 2. Lapilli 3. Ash/tuff	1. Composition of all volcaniclasts present in minor amounts 2. Composition of all neritic and pelagic grains present in minor amounts 3. Texture of siliciclastic grains present in minor amounts
Mixed	1. Composition of neritic and pelagic grains present in major amounts 2. Texture of clastic grains present in major amounts	1. Mixed sediments	1. Composition of neritic and pelagic grains present in minor amounts 2. Texture of clastic grains present in minor amounts

For siliciclastic sediment, the principal name describes the texture and is assigned according to the following guidelines:

1. The Udden-Wentworth grain-size scale (Wentworth, 1922; Table 2) defines the grain-size ranges and the names of the textural groups (*gravel, sand, silt,* and *clay*) and subgroups (*fine sand, coarse silt,* etc.) that are used as the principal names of siliciclastic sediment.
2. When two or more textural groups or subgroups are present in a siliciclastic sediment, they are listed as principal names in order of increasing abundance.
3. The suffix "*-stone*" is affixed to the principal names *sand, silt,* and *clay* when the sediment is lithified. *Conglomerate* and *breccia* are used as principal names of gravels with well-rounded and angular clasts, respectively.

For volcaniclastic sediment, the principal name describes the texture. The names and ranges of three textural groups (from Fisher and Schmincke, 1984) are as follows:

1. *Volcanic breccia:* pyroclasts >64 mm in diameter.
2. *Volcanic lapilli:* pyroclasts from 2 to 64 mm in diameter; when lithified, the term "*lapillistone*" is used.

Table 2. Udden-Wentworth grain-size scale for siliciclastic sediments (Wentworth, 1922).

Millimeters		Micrometers	Phi (ϕ)	Wentworth size class	
			−20		
	4096		−12	Boulder (−8 to −12 ϕ)	
	1024		−10		
	256		−8		
	84		−6	Cobble (−6 to −8 ϕ)	
	16		−4	Pebble (−2 to −6 ϕ)	Gravel
	4		−2		
	3.36		−1.75		
	2.83		−1.5	Granule	
	2.36		−1.25		
	2.00		−1.0		
	1.58		−0.75		
	1.41		−0.5	Very coarse sand	
	1.19		−0.25		
	1.00		0.0		
	0.84		0.25		
	0.71		0.5	Coarse sand	
	0.59		0.75		
1/2	0.50	500	1.0		
	0.42	420	1.25		
	0.35	350	1.5	Medium sand	Sand
	0.30	300	1.75		
1/4	0.25	250	2.0		
	0.210	210	2.25		
	0.177	177	2.5	Fine sand	
	0.149	149	2.75		
1/8	0.125	125	3.0		
	0.106	106	3.25		
	0.068	88	3.5	Very fine sand	
	0.074	74	3.75		
1/16	0.0625	63	4.0		
	0.063	83	4.25		
	0.044	44	4.5	Coarse silt	
	0.037	37	4.75		
1/32	0.031	31	5.0		
1.64	0.0156	15.6	6.0	Medium silt	
1/128	0.0078	7.8	7.0	Fine silt	Mud
1/256	0.0039	3.9	8.0	Very fine silt	
	0.0020	2.0	9.0		
	0.00096	0.96	10.0	Clay	
	0.00049	0.49	11.0		
	0.00024	0.24	12.0		
	0.00012	0.12	13.0		
	0.00006	0.06	14.0		

3. *Volcanic ash:* pyroclasts <2 mm in diameter; when lithified, the term "*tuff*" is used.

For mixed sediment, the principal name describes the degree of consolidation, with the term "*mixed sediment*" used for unlithified sediment, and the term "*mixed sedimentary rock*" used for lithified sediment.

Major and Minor Modifiers

The principal name of a granular sediment class is preceded by major modifiers and followed by minor modifiers (preceded by the term "with") that describe the lithology of the granular sediment in greater detail (Table 1). The most common uses of major and minor modifiers are to describe the composition and textures of grain types that are present in major (>25%) and minor (10%–25%) proportions. In addition, major modifiers can be used to describe grain fabric, grain shape, and sediment color. The nomenclature for the major and minor modifiers is outlined below.

The composition of pelagic grains can be described with the major and minor modifiers *diatom(-aceous), radiolarian, spicules(-ar), siliceous, nannofossil, foraminifer, and calcareous.* The terms *siliceous* and *calcareous* are used to describe sediments that are composed of siliceous or calcareous pelagic grains of uncertain origin.

The composition of neritic grains can be described with the following major and minor modifiers:

1. *Ooid* (or *oolite*): spherical or elliptical nonskeletal particles <2 mm in diameter that have a central nucleus surrounded by a rim with concentric or radial fabric.
2. *Bioclast* (or *bioclastite*): fragment of skeletal remains (specific names such as *molluscan* or *algal* can also be used).
3. *Pellet(-al)*: fecal particles from deposit-feeding organisms.
4. *Intraclast:* reworked carbonate-rock fragment or rip-up clast.
5. *Pisolite:* spherical or ellipsoidal, nonskeletal particle, commonly >2 mm in diameter, with or without a central nucleus but displaying multiple concentric layers of carbonate.
6. *Peloid* (or *pel*): micritized carbonate particle of unknown origin.
7. *Calcareous, dolomitic, aragonitic,* and *sideritic:* used to describe the composition of carbonate muds or mudstones (micrite) of nonpelagic origins.

The texture of siliciclastic grains is described by the major and minor modifiers *gravel(-ly), sand(-y), silt(-y),* and *clay(-ey).* The composition of siliciclastic grains can be described by:

1. Mineralogy: with such modifiers as "quartz," "feldspar," "glauconite," "mica," "kaolinite," "zeolitic," "lithic" (for rock fragments), "calcareous," "gypsiferous," or "sapropelic" (for detrital clasts of calcium carbonate, gypsum, and organic matter, respectively).
2. Provenance: the source of rock fragments (particularly in gravels, conglomerates, and breccias) can be described by such modifiers as volcanic, sed-lithic, meta-lithic, gneissic, basaltic, etc.

The composition of volcaniclastic grains is described by the major and minor modifiers *lithic* (rock fragments), *vitric* (glass and pumice), and *crystal* (mineral crystals), or by modifiers that describe the compositions of the lithic grains and crystals (e.g., *feldspar* or *basaltic*). The fabric of the sediment can be described by the major modifiers *grain-supported, matrix-supported,* and *imbricated.* Generally, fabric descriptors are applied only to gravels, conglomerates, and breccias for they provide useful information on their transport history.

Chemical Sediments

Classes of Chemical Sediments

Chemical sediments are composed of minerals that formed by inorganic processes, such as precipitation from solution or colloidal suspension, deposition of insoluble precipitates, or recrystallization of detrital evaporites and siliceous, calcareous, or carbonaceous (plant) biogenic debris. They generally have a crystalline (i.e., nongranular) texture.

There are five classes of chemical sediments: carbonaceous sediments, evaporites, silicates, carbonates, and metalliferous sediments. Each class of chemical sediment has its own distinctive classification scheme. The following chemical sediments were encountered on Leg 130.

Silicates and Carbonates

Silicates and carbonates are defined as sedimentary rocks that are nongranular and nonbiogenic in appearance and composed of silicate and carbonate minerals. Silicates and carbonates may have formed from the recrystallization of siliceous and calcareous grains, but they are distinguished by the absence of clearly identifiable granular and biogenic components. They may also form as primary precipitates, as in the case of dolomite or proto-dolomite or as hydrothermal alteration products, such as in the case of zeolites. They are classified according to their mineralogy, using principal names such as chert (microcrystalline quartz), calcite, and dolomite. They should also be modified with terms that describe their crystalline (as opposed to granular) nature, such as crystalline, microcrystalline, massive, and amorphous.

Grain Size Analyses

Bulk grain-size analyses were conducted on approximately one sample per section on unconsolidated APC cores. These results are presented in tabular and graphic form in each site report. The analyses were conducted using an eight-channel Lasentec Lab-Tec 100 particle-size analyzer. Data were collected at the following size intervals: <4, 4–8, 8–16, 16–32, 32–63, 63–125, 125–250, and >250 μm. Standard dispersal techniques were used to disaggregate the samples for analysis.

BIOSTRATIGRAPHY

Preliminary age assignments were established primarily on core-catcher samples. Samples from within the cores were examined when a critical shipboard age determination was necessary. Four microfossil groups were examined for biostratigraphic purposes: calcareous nannofossils, planktonic foraminifers, radiolarians, and diatoms. Benthic foraminifers provided preliminary paleoenvironmental information. Sample position and the abundance, preservation, and age or zone for each fossil group were recorded on the barrel sheets for each core.

Time scales by Berggren et al. (1985a, 1985b) for the Cenozoic and Kent and Gradstein (1985) for the Cretaceous provide the correlation between magnetostratigraphy and absolute time used in this report. Tables 3, 4, and 5 summarize the nannofossil, planktonic foraminifers, and diatom datums, respectively, used for Leg 130. Figures 7 and 8 show the correlation of Cenozoic chronostratigraphy, biostratigraphy, and magnetostratigraphy used for Leg 130.

Calcareous Nannofossils

The chief purpose of Leg 130 was to recover sedimentary sequences that represent a continuous stratigraphic column encompassing the interval from the present to the Lower Creta-

Table 3. Calcarous nannofossil species events and their assigned age estimates.

Event	Species	Zone (top)	Age (Ma)	References
OA	*Emiliania huxleyi*		0.09	1
FO	*Emiliania huxleyi*	NN20	0.28	1
LO	*Pseudoemiliania lacunosa*	NN19	0.46	1
LO	*Reticulofenestra asanoi*		0.83	2
FO	*Gephyrocapsa parallela*		0.90	2
FO	*Reticulofenestra asanoi*		1.06	2
LO	large *Gephyrocapsa*		1.10	2
LO	*Helicosphaera sellii*		1.19	2
FO	large *Gephyrocapsa*		1.36	2
LO	*Calcidiscus macintyrei*		1.45(1.57)	3(2)
FO	*Gephyrocapsa oceanica*		1.57	2
FO	*Gephyrocapsa caribbeanica*		1.66	2
Pleistocene/Pliocene boundary			1.66	4
LO	*Discoaster brouweri*	NN18	1.89	3
LO	*Discoaster triradiatus*		1.89	3
OA	*Discoaster triradiatus*		2.07	5
LO	*Discoaster pentaradiatus*	NN17	2.35	3
LO	*Discoaster surculus*	NN16	2.41	3
LO	*Reticulofenestra ampla*		2.62	2
LO	*Discoaster tamalis*		2.65	3
LO	*Sphenolithus* spp.		3.45	3
LO	*Reticulofenestra pseudoumbilica*	NN15	3.56	3
LO	*Amaurolithus tricorniculatus*	NN14	3.7	6a
FO	*Discoaster asymmetricus*	NN13	4.1	6a
LO	*Amaurolithus primus*		4.4	6a
FO	*Ceratolithus rugosus*	NN12	4.6	3
LO	*Ceratolithus acutus*		4.6	3
FO	*Ceratolithus acutus*		4.9(4.85)	7
LO	*Triquetrorhabdulus rugosus*		4.9	7
Pliocene/Miocene boundary			4.9	8
LO	*Discoaster quinqueramus*	NN11	5.0	7
LO	*Amaurolithus amplificus*		5.4	9
FO	*Amaurolithus amplificus*		6.0	9
FO	*Amaurolithus primus*		6.7	9
FO	*Discoaster quinqueramus*	NN10	7.5	7
FO	*Discoaster berggrenii*		8.2	6a
LO	*Discoaster hamatus*	NN9	8.7	7
LO	*Catinaster* spp.		8.8	7
FO	*Discoaster neohamatus*		9.0	7
FO	*Catinaster calyculus*		10.0	6a
FO	*Discoaster hamatus*	NN8	10.5	7
FO	*Catinaster coalitus*	NN7	11.1	7
FO	*Discoaster kugleri*	NN6	12.2	7
LO	*Coronocyclus nitescens*		12.8	9
LO	*Cyclicargolithus floridanus*		13.1	7
LO	*Sphenolithus heteromorphus*	NN5	13.6	7
LO	*Helicosphaera ampliaperta*	NN4	16.0	6a
TA	*Discoaster deflandrei* group		16.1	9
FO	*Sphenolithus heteromorphus*		18.6	7
LO	*Sphenolithus belemnos*	NN3	18.8	7
LO	*Triquetrorhabdulus carinatus*	NN2	19.5	7
FO	*Sphenolithus belemnos*		20.0	7
FO	*Discoaster druggii*	NN1	23.6	7
TA	*Sphenolithus delphix*		23.6	10
Miocene/Oligocene boundary			23.7	6a
OA	*Sphenolithus delphix*		24.7	10
LO	*Sphenolithus ciperoensis*		25.2	6b
OA	*Triquetrorhabdulus carinatus*		27.0	10
LO	*Sphenolithus distentus*	NP24	27.5(28.2)	10(6b)
AS	*S. ciperoensis/S. distentus*		28.8	10
FO	*Sphenolithus ciperoensis*	NP23	30.2	6b
FO	*Sphenolithus distentus*		34.2	6b
LO	*Reticulofenestra umbilica*	NP22	33.8(34.2)	11(6b)
LO	*Ericsonia formosa*	NP21	34.9	11
Oligocene/Eocene boundary			36.6	6b
LO	*Discoaster saipanensis*	NP20	37.7	11
LO	*Discoaster barbadiensis*		37.0	11
FO	*Chiasmolithus oamaruensis*	NP17	39.8	6b
LO	*Chiasmolithus grandis*		40.0	6b
LO	*Chiasmolithus solitus*	NP16	42.3	6b
FO	*Dictyococcites hesslandii*		42.9	11
LO	*Nannotetrina* spp.		44.2	11
FO	*Reticulofenestra umbilica* (>14 μm)		44.4	11
LO	*Chiasmolithus gigas*		47.0	6b
FO	*Chiasmolithus gigas*		48.8	12
FO	*Nannotetrina fulgens*	NP14	49.5	12

Table 3 (continued).

Event	Species	Zone (top)	Age (Ma)	References
Oligocene/Eocene boundary (Cont.)				
LO	*Discoaster sublodoensis*		49.7	12
FO	*Nannotetrina* spp.		50.3	12
LO	*Discoaster lodoensis*		50.4	12
FO	*Discoaster sublodoensis*	NP13	52.3	12
LO	*Tribrachiatus orthostylus*	NP12	54.0	12
FO	*Discoaster lodoensis*	NP11	55.0	12
FO	*Sphenolithus radians*		56.0	12
AS	*T. orthostylus-T. contortus*	[a]NP10	56.2	12
Eocene/Paleocene boundary			[b]56.4	
FO	*Triquetrorhabdulus contortus*		56.5	12
FO	*Triquetrorhabdulus bramlettei*	NP9	56.7	12
FO	*Discoaster diastypus*		56.7	12
FO	*Rhomboaster* spp.		56.8	12
LO	*Fasciculithus* spp.		56.9	12
LO	*Ericsonia robusta*		57.8	12
FO	*Campylosphaera eodela*		58.2	6b
FO	*Discoaster multiradiatus*	NP8	59.0	12
FO	*Discoaster okadai*		59.3	12
FO	*Discoaster nobilis*		59.4	12
LO	*Heliolithus kleinpellii*		60.1	12
FO	*Discoaster mohleri*	NP6	60.2	12
LO	*Chiasmolithus danicus*		61.0	6b
FO	*Heliolithus kleinpellii*	NP5	61.0	12
FO	*Heliolithus cantabriae*		61.5	12
LO	*Fasciculithus pileatus*		61.8	12
LO	*Cruciplacolithus tenuis*		61.8	6b
FO	*Fasciculithus* spp.		62.4	12
FO	*Ellipsolithus macellus*	NP3	62.8	12
FO	*Sphenolithus* spp.		62.9	12
FO	*Chiasmolithus danicus*	NP2	64.8	6b
FO	*Cruciplacolithus tenuis*	NP1	65.9	6b
FO	*Cruciplacolithus primus*		66.1	6b
Tertiary/Cretaceous boundary			66.4	6b

Notes: FO = first occurrence, LO = last occurrence, OA = onset acme, TA = termination acme, and AS = abundance shift. Zonal codes are those of Martini (1971). Age column references represent (1) Thierstein et al., 1977; (2) Sato et al., 1991; (3) Backman and Shackleton, 1983; (4) Rio et al., in press; (5) Backman and Pestiaux, 1986; (6a) Berggren et al., 1985a; (6b) Berggren et al., 1985b; (7) Backman et al., 1990; Zijderveld et al., 1986; (9) Rio et al., 1990; (10) Fornaciari et al., 1990; (11) Backman, 1987; (12) Backman, 1986.

[a] Martini (1971) defined the top of NP10 by the LO of *T. contortus*. A proclivity to diagenetic overgrowth in combination with a subtle evolutionary transition into the descendant species *T. orthostylus* prevents precise determination of the NP10/NP11 boundary. The abundance cross-over between these closely related forms, however, provides a biostratigraphic indication that is easier to recognize than the LO of *T. contortus*.

[b] Berggren et al. (1985b) originally suggested that the Eocene/Paleocene boundary is coincident with the biostratigraphic NP9/NP10 boundary, and provided an age estimate of 57.8 Ma for these two boundaries. Subsequent developments in late Paleocene/early Eocene biochronology indicate that the NP9/NP10 boundary is about 56.7 Ma (Backman, 1986), an estimate that was derived using the geomagnetic polarity history of Berggren et al. (1985b). Aubry et al. (1988) recently argued that the Eocene/Paleocene boundary does not fall at the NP9/NP10 boundary but well within NP10. Aubry and others consequently conclude that Berggren's et al. (1985b) estimate of 57.8 Ma is too old (by 0.7 m.y. in their opinion). Our biochronology in the pertinent interval differs from that of Aubry and others; however, we have adopted their argument that the Eocene/Paleocene boundary is associated with the middle to upper part of Zone NP10 (see their text on p. 735 and fig. 6). For these reasons, we will use an age of 56.4 Ma for the Eocene/Paleocene boundary.

ceous. In terms of calcareous nannofossil biostratigraphy, the classification of Leg 130 sediments was expressed through a single Cenozoic zonal scheme. Cretaceous sediments were classified biostratigraphically using a composite zonal scheme.

Chronological Framework

The age estimates of calcareous nannofossil zonal boundaries, or marker events, have been derived largely from the geomagnetic polarity time scale (GPTS) of Berggren et al. (1985a, 1985b). Their polarity history covers the time interval from the present to 84 Ma (termination of Chron 34). The GPTS of Kent and Gradstein (1985) was used in the Cretaceous time interval

Table 4. Cenozoic planktonic foraminifer species events.

Event	Species	Zone (top)	Age (Ma)
LO	*Globorotalia tosaensis*		0.6
FO	*Pulleniatina finalis*		1.3
LO	*Globigerinoides fistulosus*		1.6
Pleistocene/Pliocene boundary			1.6
FO	*Globorotalia truncatulinoides*	N21/*G. tosaensis*	1.9
LO	*Globorotalia exilis*		2.1
LO	*Globorotalia miocenica*		2.2
LO	*Globorotalia pertenuis*		2.5
LO	*Globorotalia multicamerata*		2.9
LO	*Globoquadrina altispira*		2.9
FO	*Globigerinoides fistulosus*		2.9
LO	*Sphaeroidinellopsis* spp.		3.0
FO	*Sphaeroidinella dehiscens* s.s.		3.0
FO	*Globorotalia inflata*		3.0
LO	*Globorotalia conomiozea*		3.0
FO	*Globorotalia tosaensis*	N19/*G. miocenica*	3.1
FO	*Globorotalia crassula*		3.1
FO	*Globorotalia pertenuis*		3.3
FO	*Globorotalia miocenica*		3.4
LO	*Globorotalia margaritae*		3.4
LO	*Pulleniatina primalis*		3.5
Coiling change in *Pulleniatina* (S to D)			3.8
LO	*Globigerina nepenthes*		3.9
FO	*Globorotalia crassiformis* s.s.		4.1
FO	*Globorotalia crassiformis* s.l.		4.3
FO	*Globorotalia puncticulata*		4.4
LO	*Globorotalia cibaoensis*		4.4
FO	*Sphaeroidinella dehiscens* s.l.	N18	5.1
FO	*Globorotalia tumida*		5.2
FO	*Pulleniatina spectabilis*		5.2
Pliocene/Miocene boundary			5.3
FO	*Globigerinoides conglobatus*	N17b	5.3
FO	*Globorotalia cibaoensis*	N17b	5.3
LO	*Globoquadrina dehiscens*	N17b	5.3
LO	*Globorotalia lenguaensis*	N17b	5.3
FO	*Globorotalia margaritae*		5.6
FO	*Pulleniatina primalis*	N17a	5.8
FO	*Globorotalia conomiozea*		6.1
FO	*Globorotalia plesiotumida*	N16	7.1
FO	*Neogloboquadrina dutertrei* s.l.	*N. acostaensis*	8.0
FO	*Neogloboquadrina acostaensis*	N15/*G. menardii*	10.2
LO	*Globorotalia siakensis* (= *mayeri*)	N14/*G. mayeri*	10.4
FO	*Globigerina nepenthes*	N13	11.3
LO	*G. fohsi lobata* and *G. fohsi robusta*	N12	11.5
FO	*Globorotalia fohsi robusta*		12.6
FO	*G. fohsi lobata* (= *G. fohsi fohsi*)	N11	13.1
FO	*Globorotalia praefohsi*	N10	13.9
LO	*Globorotalia peripheroronda*		14.6
FO	*Globorotalia peripheroacuta*	N9/*G. peripheroronda*	14.9
LO	*Praeorbulina sicana*	N9/*G. peripheroronda*	14.9
LO	*Praeorbulina glomerosa*	N9/*G. peripheroronda*	14.9
FO	*Orbulina suteralis*	N8/*P. glomerosa*	15.2
FO	*Praeorbulina glomerosa*	*G. insueta*	16.3
FO	*Praeorbulina sicana*	N7	16.6
FO	*Globorotalia miozea*		16.8
LO	*Globorotalia zealandica*		16.8
FO	*Globorotalia birnageae*		17.0
LO	*Catapsydrax stainforthi*		17.4
FO	*Globorotalia zealandica*	N6/*C. stainforthi*	17.6
LO	*Globorotalia incognita*	N6/*C. stainforthi*	17.6
LO	*Catapydrax dissimilis*	N6/*C. stainforthi*	17.6
FO	*Globorotalia praescitula*		17.7
FO	*Globigerinatella insueta*	N5	19.0
FO	*Globigerinoides altiaperturus*		20.9
LO	*Globorotalia kugleri* s.s.	N4/*G. kugleri*	21.8
FO	*Globoquadrina dehiscens*		23.2
FO	*Globorotalia incognita*		23.2
LO	*Globigerina angulisuteralis*		23.2
LO	*Globorotalia pseudokugleri*		23.2
Miocene/Oligocene boundary			23.7
FO	*Globorotalia kugleri* s.s.	P22/*G.ciperoensis*	23.7
FO	*Globigerinoides primordius* (common)		24.5
FO	*Globigerinoides primordius* (rare)		25.8
FO	*Globorotalia pseudokugleri*		[b]26.3
LO	*Globorotalia opima*	P21b/*G. opima*	28.2
LO	*Chiloguembelina* spp.	P21a	30.0
FO	*Globigerina angulisuturalis*	P20	[b]31.6
LO	*Globigerina angiporoides*		32.0

Table 4 (continued).

Event	Species	Zone (top)	Age (Ma)
Miocene/Oligocene boundary (Cont.)			
FO	*Globigerina opima*	*G. ampliapertura*	32.7
LO	*Globigerina ampliapertura*	P19	[b]32.8
LO	*Pseudohastigerina* spp.	P18/*C. chip.-P. micra*	34.0
Oligocene/Eocene boundary			36.6
LO	*Globorotalia cocoaensis*	P17/*G. cerroazulensis*	[b]36.6
LO	*Globorotalia cerroazulensis*	*G. cerroazulensis*	36.6
LO	*Hantkenina* spp.	*G. cerroazulensis*	36.6
LO	*Globigerapsis* spp.		37.0
LO	*Cribrohantkenina inflata*	P16	[b]37.2
LO	*Porticulasphaera semiinvoluta*	*P. semiinvoluta*	37.6
FO	*Cribrohantkenina inflata*	P15	[b]38.1
LO	*Acarinina* and *Truncorotaloides rohri*		40.6
LO	*Morozovella spinulosa*		41.1
FO	*Porticulasphaera semiinvoluta*	P14/*T. rohri*	41.3
LO	*Subbotina frontosa*		42.0
LO	*Globigerapsis beckmanni*	P13/*G. beckmanni*	42.6
FO	*Globigerapsis beckmanni*	P12/*M. lehneri*	43.0
LO	*Acarinina bullbrooki*	P12/*M. lehneri*	43.0
FO	*Globorotalia pomeroli*		44.7
FO	*Globigerapsis index*		45.0
FO	*Morozovella lehneri*	P11/*G. subconglobata*	46.0
LO	*Morozovella aragonensis*	P11/*G. subconglobata*	46.0
FO	*Globigerapsis kugleri*	P10/*H. aragonensis*	[a]49.0
FO	*Hantkenina* spp.	P9/*A. pentacamerata*	52.0
FO	*Planorotalites palmerae*	P8/*M. aragonensis*	53.4
FO	*Morozovella aragonensis*	P7/*M. formosa formosa*	[a]54.0
FO	*Morozovella formosa*	P6b/*M. subbotinae*	[a]55.2
Eocene/Paleocene boundary			56.4
LO	*Morozovella velascoensis*	P6a/*M. velascoensis*	57.8
FO	*Morozovella subbotinae*	P5	[b]58.2
LO	*Planorotalites pseudomenardii*	P4/*P. pseudomenardii*	58.8
FO	*Planorotalites pseudomenardii*	P3b/*P. pusilla pusilla*	61.0
FO	*Morozovella velascoensis*		61.7
FO	*Morozovella albeari*		61.7
LO	*Subbotina pseudobulloides*		61.7
FO	*Morozovella pusilla*	P3a/*M. angulata*	62.0
FO	*Morozovella conicotruncata*	P3a/*M. angulata*	62.0
FO	*Morozovella angulata*	P2/*M. uncinata*	62.3
FO	*Morozovella uncinata*	P1c/*S. trinidadensis*	63.0
LO	*Globastica daubjergensis*		64.0
LO	*Planorotalites compressus*	P1b/*S. pseudobulloides*	64.5
FO	*S. praecursoria (trinidadensis)*	P1b/*S. pseudobulloides*	64.5
FO	*Subbotina triloculinoides*	P1a	[b]65.5
FO	*Subbotina pseudobulloides*	Pα/*P. eugubina*	[b]66.1
FO	*Parvularugoglobigerina eugubina*		66.35
LO	*Globotruncana*		66.4

Notes: FO = first occurrence and LO = last occurrence. Most datums are from Berggren et al. (1985a, 1985b). Refer to Table 3 for comments on the placement of the Eocene/Paleocene boundary.
[a] From Aubry et al. (1988).
[b] From Berggren and Miller (1988).

older than Chron 34 (T). This particular event in time connects the two time scales. A few age estimates shown in Table 3 are taken directly from Berggren et al. (1985a, 1985b). The increasing availability of Cenozoic bio- and magnetostratigraphies in deep-sea sediments has resulted in improved correlations between nannofossil biostratigraphy and the geomagnetic polarity history, improvements that are accounted for in Table 3.

The biochronology of Cretaceous calcareous nannofossil marker events still lacks much of the detail that exists for Cenozoic markers, simply because the direct correlations between bio- and magnetostratigraphy are fewer in number in the Cretaceous. For this reason, we have only listed age assignments for Cenozoic marker events. It should be pointed out, however, that Cenozoic age estimates in many cases also are associated with serious uncertainties. One of the major reasons is the lack, or limited availability, of adequate magnetostratigraphic records from tropical/equatorial environments. As a consequence, we have few data on the bio- and magnetostratigraphic correlations from those regions in which the highest rates of taxonomic evolution have occurred; the data in Berggren et al. (1985a, 1985b), for example, predominantly represent mid-latitude estimates.

Table 5. Diatom species events and their assigned age estimates.

Event	Species	Zone (top)	Age (Ma)	References
LO	*Nitzschia reinholdii*	NTD 16	0.65	1
LO	*Rhizosolenia praebergonii* var. *robusta*		1.55	1
FO	*Pseudoeunotia doliolus*	NTD 15	1.8	1
LO	*Thalassiosira convexa* var. *aspinosa*		2.1	1
LO	*Nitzschia jouseae*		2.6	1
FO	*Rhizosolenia praebergonii*	NTD 14	3.0	1
FO	*Asteromphalus elegans*		3.9	1
LO	*Nitzschia cylindrica*		4.35	1
FO	*N. jouseae*	NTD 13	4.5	2
FO	*Thalassiosira oestrupii*		5.2 (5.1)	4
LO	*Asterolampra acutiloba*		5.35	2
LO	*Nitzschia miocenica*		5.6	2
LO	*Thalassiosira praeconvexa*		5.8	2
FO	*T. convexa* var. *aspinosa*	NTD 12	6.1	2
LO	*Nitzschia porteri*		7.2 (6.7)	2
FO	*N. miocenica*	NTD 11	7.3 (6.8)	2
LO	*Rossiella paleacea*		7.4 (6.9)	2
LO	*Coscinodiscus nodulifer* var. *cylcopus*		7.9	3
LO	*Thalassiosira burckliana*		8.0 (7.0)	2
LO	*Actinocylcus ellipticus* var. *javanica*		8.0	3
LO	*Coscinodiscus yabei*	NTD 10	8.6 (7.5)	2
FO	*T. burckliana*		9.0 (8.0)	2
LO	*Coscinodiscus temperei* var. *delicata*		9.8 (8.2)	2
LO	*C. vetustissimus* var. *javanica*		10.7 (8.5)	2
LO	*Actinocyclus moronensis*	NTD 9	11.3 (8.9)	2
LO	*Denticulopsis punctata* f. *hustedtii*		12.2 (10.7)	2
LO	*Synedra jouseana*		12.3 (12.1)	3
LO	*Craspedodidscus coscinodiscus*	NTD 8	12.2 (10.7)	2
LO	*Actinocyclus ellipticus* var. *spiralis*		12.4 (12.3)	3
FO	*Hemidiscus cuneiformis*		12.6 (11.2)	2
FO	*Coscinodiscus temperei* var. *delicata*	NTD 7	12.8	
LO	*Coscinodiscus lewisianus*	NTD 6	13.5 (12.9)	2
LO	*Denticulopsis hustedtii*		13.7	2
LO	*Cestodiscus pulchellus* var. *maculatus*		13.9	3
LO	*Cestodiscus peplum*	NTD 5	14.1	2
FO	*A. ellipticus* var. *spiralis*		14.2 (14.1)	3
LO	*Annellus californicus*		15.0	2
FO	*Actinocyclus ingens*		15.5	2
LO	*C. lewisianus* var. *similis*		15.7	3
FO	*C. peplum*	NTD 4	16.4	2
LO	*Raphidodiscus marylandicus*		16.7	3
FO	*Denticulopsis nicobarico*	NTD 3	17.8	
LO	*Craspedodiscus elegans*	NTD 2	18.7	2
LO	*Borgorovia veniamini*	NTD 1	19.9	2
LO	*C. lewisianus* var. *rhomboides*		22.5	2
FO	*Rossiella paleacea*	*Rocella gelida* Zone	22.7	2
LO	*Rocella vigilans*		22.7?	3
FO	*B. veniamini*		24.0?	3
LO	*Coscinodiscus excavatus*	*C. excavatus*	33.0?	3

Notes: FO = first occurrence and LO = last occurrence. Zonal codes are those of Barron (1985). Age column references represent (1) Barron, 1985a; (2) summary in Barron et al., 1985a; (3) Barron et al., 1985b; (4) Baldauf, 1985.

Cenozoic Zonation

From the zonal schemes available for the subdivision of nannofossils in Cenozoic sediments, we chose the scheme of Martini (1971). This scheme does not represent the ultimate resolution (e.g., the number of evolutionary appearances/disappearances per unit time) that can be achieved in Cenozoic deep-sea sediments, because deep-sea biostratigraphy has developed rapidly over the past two decades and continues to do so. Yet this zonal scheme does provide a simple picture of biostratigraphic relationships in the cored sequences. The fact that most marine

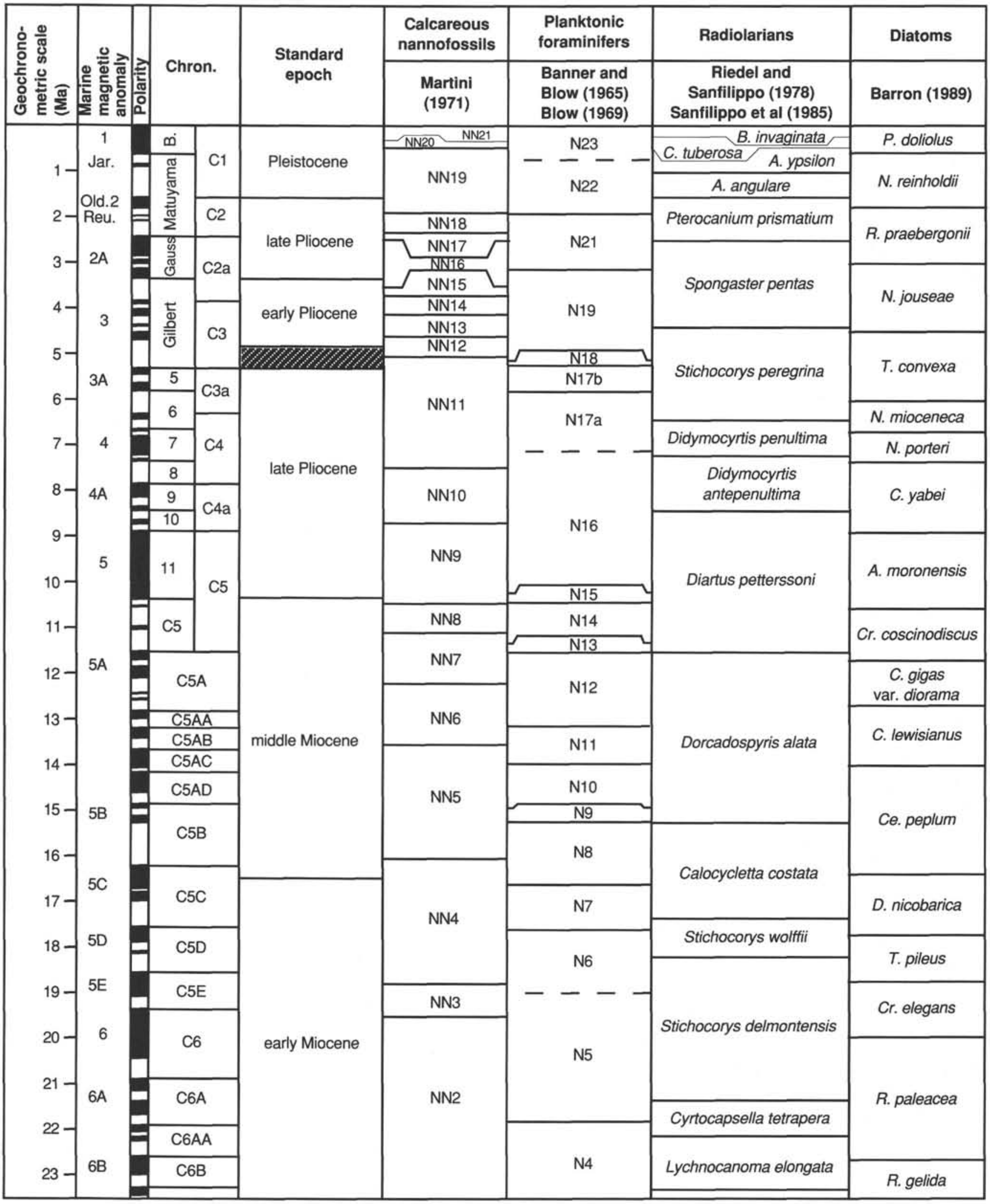

Figure 7. Correlation of Neogene chronostratigraphy, biostratigraphy, and magnetostratigraphy used during Leg 130. Magnetic chron terminology follows that adopted by Leg 108 (Shipboard Scientific Party, 1988a). Correlation of the magnetic polarity record, epoch boundaries, and planktonic foraminifer zones follows Berggren et al. (1985b). Nannofossil zonal boundaries are based on datums presented in Table 3. Correlation of the late Miocene–Pleistocene radiolarian zones with the magnetic polarity record follows Shipboard Scientific Party (1989a). Correlation of the early Miocene–middle Miocene radiolarian zones with the magnetic polarity record follows Barron (1989). Diatom events are presented in Table 3. Correlation of diatom zones with magnetic polarity follows Barron (1989). The hatchured area at the Miocene/Pliocene boundary shows that the range in age of the boundary is between 5.3 (Berggren et al., 1985b) and 4.9 Ma (Zijderveld et al., 1986).

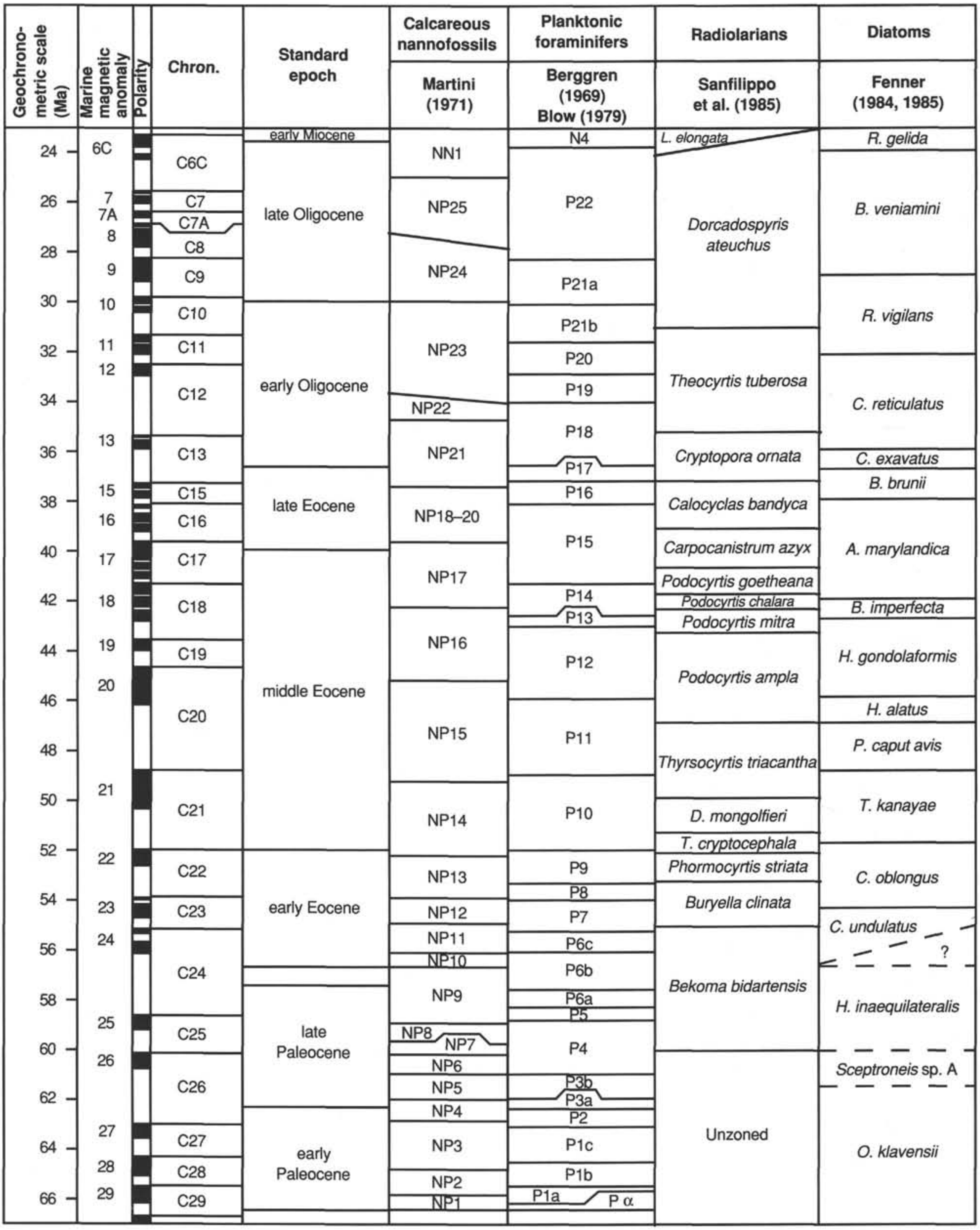

Figure 8. Correlation of Paleogene chronostratigraphy, biostratigraphy, and magnetostratigraphy used during Leg 130. Hatchured area at the Paleocene/Eocene boundary shows that range in age of the boundary is between 57.7 (Berggren et al., 1985a) and 56.4 Ma (Table 3). Correlation of the magnetic polarity record, epoch boundaries, and planktonic foraminifer zones follows Berggren et al. (1985a), as modified by Aubry et al. (1988) and Berggren and Miller (1988). Nannofossil zonal boundaries are based on the datums presented in Table 3. Correlation of radiolarian zones follows Berggren et al. (1985a) and Barron (1989) for the Oligocene, and Aubry et al. (1988) for the Eocene and Paleocene. Diatom zonation is correlated with nannofossil and radiolarian zones following Fenner (1984) and Bolli et al. (1985, chapter 2).

geologists are familiar with Martini's scheme also adds to its value as an initial framework for Leg 130 nannofossil biostratigraphy.

We have, however, also used numerous biostratigraphic events that are not in Martini's (1971) zonal boundary definitions (Table 3). These additional events represent a resource that creates a substantially improved biostratigraphic and biochronologic resolution, which becomes important, for example, in the reconstruction of Cenozoic sediment accumulation rates. In this context, it should be emphasized that many arguments can be raised for continuous revision and further subdivision of existing zonal schemes, including Martini's scheme, but it is likewise important to emphasize that this approach invariably leads to an infinitely growing set of code systems and/or code numbers.

Cretaceous Zonation

The zonations of Sissingh (1977) and Thierstein (1976) were used together with the Berggren et al. (1985c) GPTS from the Cretaceous/Tertiary boundary to the termination of Chron 34, and beyond there together with the Kent and Gradstein (1985) GPTS.

Methods

Calcareous nannofossils were examined by means of standard light microscope techniques (under crossed nicols or transmitted light at about 790×, or 1250×, magnification).

A peculiar characteristic among calcareous nannofossil assemblages is that individual samples may show signs of strong etching as well as strong overgrowth; more dissolution-resistant forms simply add secondary calcite provided by more dissolution-prone morphotypes. Qualitative descriptions of calcareous nannofossil preservational states commonly involve a sophisticated code system that accounts for dissolution and overgrowth on a progressive scale (e.g., Roth and Thierstein, 1972). When considering the purposes of the shipboard descriptions, and the Leg 130 water depth range, we have adopted the simplest possible, but nevertheless effective, code system for characterizing preservational states. Thus, preservation was recorded with one of the following three letter designations:

G = good (little or no evidence of dissolution and/or secondary overgrowth of calcite; diagnostic characteristics fully preserved);
M = moderate (dissolution and/or secondary overgrowth; partially altered primary morphological characteristics; however, nearly all specimens can be identified at the species level); and
P = poor (severe dissolution, fragmentation, and/or secondary overgrowth with primary features largely destroyed; many specimens cannot be identified at the species and/or generic level).

Five different levels of relative abundance were defined as follows:

A = abundant (the taxonomic category comprises >10% of the total assemblage);
C = common (the taxonomic category comprises from 1% to 10% of the total assemblage);
F = few (the taxonomic category comprises from 0.1% to 1.0% of the total assemblage); and
R = rare (the taxonomic category comprises <0.1% of the total assemblage); and
B = barren.

Planktonic Foraminifers

Zonation

Berggren et al. (1985a, 1985b) present the most comprehensive compilation of Cenozoic planktonic foraminifer zonal schemes and their correlation with magnetostratigraphy and the geochronometric time scale. The Paleogene has subsequently been modified by Aubry et al. (1988) and Berggren and Miller (1988). Table 4 presents a list of planktonic foraminifer first (FO) and last (LO) occurrence datums for the Cenozoic based on these studies.

In the Neogene, we primarily followed the zonal scheme of Blow (1969) ("N" zones), as modified by Kennett and Srinivasan (1983). Species datum levels of Berggren et al. (1985c) were used for the purpose of assigning absolute age estimates to zonal boundaries (Table 4). However, we note two modifications to the placement of the "N" zonal boundaries on Figure 2 of Berggren et al. (1985c) depicting the compilation of Neogene geochronology: (1) the N19/N21 boundary was placed at 3.1 Ma, based on the FO of *Globorotalia tosaensis;* and (2) the N11/N12 boundary was placed at 13.1 Ma, based on the FO of *Globorotalia fohsi.*

We followed Berggren et al. (1985c) in placing the Pliocene/Pleistocene boundary at the top of the Olduvai Subchron (1.6 Ma). The FO of *Globorotalia truncatulinoides* commonly has been used to define the base of the Pleistocene (e.g., Blow, 1969; Bolli and Premoli Silva, 1973; Stainforth et al., 1975; Kennett and Srinivasan, 1983; Bolli and Saunders, 1985). Berggren et al. (1985c) placed the FO of *G. truncatulinoides* at 1.9 Ma. The Pliocene/Pleistocene boundary was recognized in the Leg 130 material by the LO of *Globigerinoides fistulosus* (1.6 Ma according to Berggren et al., 1985c). This taxon is well developed in the northern Ontong Java Plateau area. The co-occurrence of *G. fistulosus* and *G. truncatulinoides* defined the uppermost Pliocene part of Zone N22.

Within the Pliocene, a coiling change in the genus *Pulleniatina* (sinistral to dextral) was used to separate undifferentiated Zones N19–N20 from undifferentiated Zones N18–N19. We did not recognize *Globorotalia pseudopima,* used by Blow (1969) to define the base of Zone N20, in material recovered during Leg 130. In the lower Pliocene, *Sphaeroidinella dehiscens* s.l. occurred only rarely and sporadically in Leg 130 material; therefore, it was not possible to separate Zones N18 and N19 consistently. Some workers have used the total range of *Globorotalia margaritae* to define the lower Pliocene interval (e.g., Bolli and Premoli Silva, 1973; Stainforth et al., 1975; Bolli and Saunders, 1985). Berggren et al. (1985c) placed the FO of *G. margaritae* at 5.6 Ma (uppermost Miocene). We placed the Miocene/Pliocene boundary at the LO of *Globoquadrina dehiscens* and the FO of *Globorotalia tumida.*

The placement of the Oligocene/Miocene boundary based on planktonic foraminifers has experienced a long history of interpretation and varied application (see reviews by Berggren et al., 1985c; Berggren and Miller, 1988). Kennett and Srinivasan (1983) used the FO of *Globoquadrina dehiscens* to mark the boundary for both tropical and temperate zonations. Berggren et al. (1985c) used the FO of *Globorotalia kugleri* s.s., citing the FO of *G. dehiscens* slightly subsequent to that of *G. kugleri* in the stratotype of the Aquitanian Stage. Berggren and Miller (1988) noted that the FO of *G. dehiscens* is about 0.5 m.y. after the FO of *G. kugleri* s.s. Therefore, the FO of *G. dehiscens* also is useful for approximating the Oligocene/Miocene boundary, as suggested by Kennett and Srinivasan (1983, p. 184) and Berggren et al. (1985c, p. 219); however, this taxon occurs only sporadically in the basal Miocene material recovered during Leg

130. The problem in using the *G. kugleri* datum has stemmed from differentiating between *G. kugleri* s.l. (including *G. pseudokugleri* and *G. mendacis*) and *G. kugleri* s.s. In this report, we followed Berggren et al. (1985c) in using the FO of *G. kugleri* s.s. to define the Oligocene/Miocene boundary (P22/N4).

In the Paleogene, we primarily followed the zonal scheme of Berggren (1969) and Blow (1979) ("P" Zones), as recently modified by Berggren and Miller (1988).

For the Cretaceous, the zonal schemes of Caron (1985) and Sliter (1989) were used. Sliter (1989) has correlated the zones with the magneto-geochronology of Kent and Gradstein (1985). It should be noted that substage boundaries, and especially biostratigraphic zonal boundaries, are fixed poorly with the geochronometric time scale.

Methods

Unlithified ooze was soaked briefly in a weak Calgon solution and afterward was washed directly over a 63-μm mesh sieve and dried. Semilithified ooze and chalk was first broken up by hand and soaked in a weak Calgon solution; afterward, these samples were washed over a 63-μm mesh sieve and dried. Large chunks of dried chalk were crushed with a pestle first and then processed a second time. The samples were again soaked in a weak Calgon solution, placed in an ultrasonic bath for about 1 min, and then washed over a 63-μm mesh sieve and dried. The extraction of foraminifers from limestone was difficult, but some success has resulted from crushing the rock first using a Carver hydraulic press. The crushed limestone was ground up even finer with the mortar and pestle. The fine sediment was then soaked in a hot Calgon solution, placed in an ultrasonic bath for about 1 min, and washed over a 63-μm mesh sieve and dried. The crushing method was particularly successful using limestones with obvious clay or ash content.

Planktonic species abundances were estimated (no actual counts were made) using the following categories:

R = rare (<3%);
F = few (3%–15%);
C = common (15%–30%); and
A = abundant (>30%).

Preservational characteristics were divided into three categories:

G = good (>90% of the specimens unbroken);
M = moderate (30%–90% of the specimens showing dissolved or broken chambers); and
P = poor (with samples dominated by fragments and specimens with broken or dissolved chambers).

Benthic Foraminifers

Core-catcher samples for benthic foraminifers were processed by wet sieving through a 63-μm mesh screen and drying the sand fraction on a hot plate. Sediment treatment methods before sieving varied with the amount of consolidation of the calcareous ooze, as described under the section on planktonic foraminifers. Because the low frequency of benthic specimens relative to planktonic microfossils makes any estimate of species content difficult, census data were prepared on representative samples of various ages; their principal taxa are listed in the site reports. These data are mostly based on counts of 100–300 specimens portioned from the sample by microsplitter. The intent of this census is to present an overview of the changes in the benthic assemblages through time along the plateau transect and to provide a background for detailed studies of the paleobathymetric history of the plateau and its paleoceanographic record.

The generic classification of Loeblich and Tappan (1987) was used where possible. Pacific modern and fossil deep-water benthic species are identified in the works of Douglas (1973), Burke (1981), Resig (1981), Thomas (1985), van Morkhoven et al. (1986), and Hermelin (1989).

Radiolarians

Zonation

During Leg 130, the low-latitude zonations of Sanfilippo et al. (1985) and Saunders et al. (1984) were used for the Cenozoic. Zonations proposed by Sanfilippo and Riedel (1985) were used for the Cretaceous. Radiolarian species events published by Riedel and Sanfilippo (1978), Sanfilippo et al. (1985), and Shipboard Scientific Party (1989a) were used to establish a biochronology for Leg 130.

Methods

For most upper Neogene samples, the standard treatment with hydrochloric acid and hydrogen peroxide, as described by Sanfilippo et al. (1985), was applied. This procedure did not disaggregate radiolarians from the pelagic clay matrix in most middle Miocene and older samples. For these samples, several cubic centimeters of sediment were placed in a 400-ml beaker and 2 teaspoons of Calgon were added, followed by the addition of hot water and 5 ml of 30% hydrogen peroxide. The sample was treated in an ultrasonic bath for about 3 min. This method was especially essential for cleaning Cretaceous radiolarians. Paleogene and Cretaceous limestones were crushed using a Carver hydraulic press. Some of these samples were ground further with a mortar and pestle (see also foraminifer methods above). All samples were sieved with 63-μm mesh stainless sieve. Strewn slides were prepared to examine the radiolarians.

The abundance recorded is based on qualitative examinations. The following criteria were used:

A = abundant (>100 specimens);
C = common (50–100 specimens);
F = few (5–50 specimens); and
R = rare (<5 specimens).

The preservation states of radiolarians were defined as follows:

G = good (no sign of dissolution);
M = moderate (minor dissolution); and
P = poor (strong dissolution).

Diatoms

Zonation

Significant contributions to the understanding of the Neogene diatom biostratigraphy from the equatorial Pacific include studies by Burckle (1972) and Barron (1985b), among others. The low-latitude diatom zonation used for Leg 130 is that proposed by Barron (1985b) and Barron et al. (1985a, 1985b) for the upper Oligocene through Holocene sequence in the central equatorial Pacific, and the low-latitude zonation summarized by Fenner (1985) for the Upper Cretaceous through Oligocene sequence. Diatom species events published by Baldauf (1985), Barron (1985a), and Barron et al. (1985a, 1985b) were used on Leg 130 and are summarized in Table 5.

Methods

Each core-catcher sample (approximately 10 cm^3 of sediment) was processed in a 400-ml beaker with hydrogen peroxide and hydrochloric acid, using heat to speed the chemical reaction. The sample was then diluted by adding 300 ml of distilled water and decanted after settling for 2 hr. The dilution/decanting process was repeated until a pH of 6 was reached. The preparation of Cretaceous samples was the same as for radiolarians (see above), although the sample was not sieved. Strewn slides of acid-cleaned material were prepared on 22- × 50-mm cover glasses and mounted on glass slides using Hyrax or Piccolyte mounting media. They were examined with a Zeiss compound microscope under Phase Contrast illumination at 500× to check for the presence of biostratigraphic marker species. The identification of species was routinely checked at 1250×.

Species were considered abundant (A) when two or more specimens were present in one field of view at 500×; common (C) if one specimen was encountered in two fields of view; few (F) if one specimen was observed in one horizontal traverse across the slide; and rare (R) if less than one was observed per traverse. If no diatoms were encountered, the sample was recorded as barren.

The preservation of diatoms was classified according to three major categories based on the presence of complete or broken, thinly to heavily silicified valves, as follows:

G = good, well-preserved specimens, thinly silicified valves present, only minor signs of dissolution or even none at all;
M = moderate, some thinly silicified valves present, slight to moderate dissolution; and
P = poor, only heavily silicified valves present, abundant broken specimens, severe dissolution.

The criteria for distinguishing whole from partial diatoms follow Schrader and Gersonde (1978).

PALEOMAGNETICS

Paleomagnetic studies on Leg 130 measured the natural remanent magnetization (NRM) and the remanence after stepwise demagnetization of continuous sections of the archive half-core in both sediments and basement. Alternating field (AF) demagnetization was applied to half-core sections with NRM measurements that indicated probable stable remanence and intensity levels above the lower operational limit of the shipboard cryogenic magnetometer (about 0.01 mAm^{-1}). Demagnetization allowed directions of the characteristic remanent (primary) magnetization (ChRM) to be isolated from the NRM of both sediments and igneous rocks by removing secondary components, predominantly viscous remanent magnetizations (VRMs), and magnetizations acquired during drilling.

Measurement of the ChRM fulfilled two complementary purposes. First, magnetic polarity throughout the sediment column was determined to allow the construction of a magnetostratigraphy. Reference was made to the magnetostratigraphies of Berggren et al. (1985b) and Kent and Gradstein (1985) (Tables 6 and 7). Second, the direction of the ChRM provided a history of the motion of the Ontong Java Plateau in the geomagnetic reference frame. Declinations from unoriented cores are indeterminate, so these cores could only contribute paleoinclinations, from which paleolatitudes were directly calculated. Paleoinclinations from Pliocene to Eocene sites were too low and scattered to allow a clear distinction of individual measurements into normal and reversed sets, so direct calculation of paleoinclinations was not possible; instead, the frequency distribution of inclination was plotted, and peaks in this distribution sought.

Table 6. Geomagnetic polarity time scale for the Cenozoic and Late Cretaceous (after Berggren et al., 1985a, 1985b, 1985c).

Normal polarity interval (Ma)	Anomaly	Normal polarity interval (Ma)	Anomaly
0–0.73	1	23.55–23.79	6C
0.91–0.98		24.04–24.21	6C
1.66–1.88	2	25.50–25.60	7
2.02–2.04		25.67–25.97	7
2.12–2.14		26.38–26.56	7A
2.47–2.92	2A	26.86–26.93	8
2.99–3.08	2A	27.01–27.74	8
3.18–3.40	2A	28.15–28.74	9
3.88–3.97	3	28.80–29.21	9
4.10–4.24	3	29.73–30.03	10
4.40–4.47	3	30.09–30.33	10
4.57–4.77	3	31.23–31.58	11
5.35–5.53	3A	31.64–32.06	11
5.68–5.89	3A	32.46–32.90	12
6.37–6.50		35.29–35.47	13
6.70–6.78	4	35.54–35.87	13
6.85–7.28	4	37.24–37.46	15
7.35–7.41	4	37.48–37.68	15
7.90–8.21	4A	38.10–38.34	16
8.41–8.50	4A	38.50–38.79	16
8.71–8.80		38.83–39.24	16
8.92–10.42	5	39.53–40.43	17
10.54–10.59		40.50–40.70	17
11.03–11.09		40.77–41.11	17
11.55–11.73	5A	41.29–41.73	18
11.86–12.12	5A	41.80–42.23	18
12.46–12.49		42.30–42.73	18
12.58–12.62		43.60–44.06	19
12.83–13.01		44.66–46.17	20
13.20–13.46		48.75–50.34	21
13.69–14.08		51.95–52.62	22
14.20–14.66		53.88–54.03	23
14.87–14.96	5B	54.09–54.70	23
15.13–15.27	5B	55.14–55.37	24
16.22–16.52	5C	55.66–56.14	24
16.56–16.73	5C	58.64–59.24	25
16.80–16.98	5C	60.21–60.75	26
17.57–17.90	5D	63.03–63.54	27
18.12–18.14	5D	64.29–65.12	28
18.56–19.09	5E	65.50–66.17	29
19.35–20.45	6	66.74–68.42	30
20.88–21.16	6A	68.52–69.40	31
21.38–21.71	6A	71.37–71.65	32
21.90–22.06		71.91–73.55	32
22.25–22.35		73.96–74.01	
22.57–22.97	6B	74.30–80.17	33
23.27–23.44	6C	84.00–118.00	34

Absolute declinations were determined for cores oriented by the multishot orientation tool. Complete declination-inclination data allow the determination of an apparent polar wander path (APWP), but directly oriented data were limited to cores younger than the middle Miocene. It may prove possible to orient deeper cores by reference to VRMs acquired by these cores in the direction of the axial dipole field; this will require detailed, land-based demagnetization studies.

Discrete samples were taken as cubes in the oozes and as minidrill cores in the chalks, radiolarian silts, and basalts. Magnetization in most of the sediments was very weak, frequently <0.1 mAm^{-1}. Measurement of discrete samples, therefore, was reserved for land-based studies, for which more sensitive magnetometers would be available. Measurement of most of the archive-half cores in the basalt basement indicated a stable magnetization with little overprinting; demagnetization was restricted to a few cores with exceptional NRMs. Discrete samples of the basement rocks also were reserved for land-based studies to allow demagnetization in closely spaced stages.

Magnetic susceptibility of the half-core sections was measured as part of the physical properties package (see Tarduno et al., this volume). Measurements were collected at 3 to 10 cm intervals with a Bartington Instruments Magnetic Susceptibility

Table 7. Geomagnetic polarity time scale for the Early Cretaceous and Late Jurassic (after Kent and Gradstein, 1985).

Anomaly (reversed polarity)	Normal polarity interval (Ma)	Anomaly (normal polarity)
	84.00–118.00	Cretaceous Quiet Zone
M0	118.70–121.81	
M1	122.25–123.03	M2
M3	125.36–126.46	M4
M5	127.05–127.21	
M6	127.34–127.52	
M7	127.97–128.33	
M8	128.60–128.91	
M9	129.43–129.82	
M10	130.19–130.57	
	130.63–131.00	
	131.02–131.36	
M10N	131.65–132.53	
M11	133.03–133.08	
M11	133.50–134.01	
	134.42–134.75	
M12	135.56–135.66	
	135.88–136.24	
	136.37–136.64	
M13	137.10–137.39	
M14	138.30–139.01	
M15	139.58–141.20	
M16	141.85–142.27	
M17	143.76–144.33	
M18	144.75–144.88	
	144.96–145.98	
M19	146.44–146.75	
	146.81–147.47	
M20	148.33–149.42	
M21	149.89–151.46	
	151.51–151.56	
	151.61–151.69	
M22	152.53–152.66	
	152.84–153.21	
	153.49–153.52	
M23	154.15–154.48	
	154.85–154.88	
M24	155.08–155.21	
	155.48–155.84	
	156.00–156.29	
M25	156.55–156.70	
	156.78–156.88	
	156.96–157.10	
	157.20–157.30	
	157.38–157.46	
	157.53–157.61	
	157.66–157.85	
PM26	158.01–158.21	
PM27	158.37–158.66	
PM28	158.87–159.80	
PM29	160.33–(169.00)	Jurassic Quiet Zone

Meter (Model MS1, using a MS1/CX, 80-mm, whole-core sensor loop set to 0.47 kHz). Severe drift problems with the existing susceptibility loop required its replacement during Leg 130. Signal clipping was found to be a problem with many of the weakly magnetized sediments on the "1" sensitivity range; when there was an indication that this was obscuring a real signal, sensitivity was switched to "0.1".

Instruments

Magnetic remanence on Leg 130 was measured with the shipboard 2-G Enterprises (Model 760R), three-axis, pass-through cryogenic superconducting rock magnetometer, which is integrated with an on-line AF demagnetizer (Model 2G600) capable of alternating fields as high as 25 mT. ODP policy limits demagnetization of the archive half-core to 15 mT or the mean destructive field, whichever is the smaller. Communications between superconducting quantum interference devices (SQUIDs), the AF degaussing system, and the drive motor were linked through a FASTCOM4 multiserial communications board in an IBM PC-AT compatible computer. All devices and actual measurements of archive half-cores were controlled by a modified version of the Rhode Island University BASIC program. Program commands enable the magnetometer to operate at the 1× scale with flux counting for weakly magnetized sediments and 100× for basement. Some calibration error may occur at the 100× scale, resulting in incorrect declinations and inclinations; comparative calibration between the 1× and 100× scales on Leg 123 (Shipboard Scientific Party, 1990a, p. 46) showed this error to be <5%.

The SQUID sensors in the cryogenic magnetometer measured magnetization over an interval approximately 15 cm long. Each axis has a slightly different response curve. The widths of the sensor regions imply that as much as 150 cm^3 of core contributes to the sensor signals. The large volume of core material within the sensor region permits an accurate determination of remanence for weakly magnetized cores despite the high background noise levels related to the ship's motion. Declinations and inclinations are best determined by deconvolution of the x,y,z data. No deconvolution program was available on Leg 130, however, so declination and inclination were calculated directly from the x,y,z data; on the other hand, intensity was calculated by dividing the magnetic moment by the volume of the sample within the sensors (i.e., the length within the sensor region by the cross-sectional area of the core).

Sediments

Remanence measurements of sediments were performed by passing continuous archive-half core sections through the cryogenic magnetometer. Depending on the resolution desired and on the backlog of cores to be processed, measurements were taken at 1-, 3-, 5-, or 10-cm spacings. Demagnetization was normally carried out at 15 mT.

Basalt

Basaltic rocks were measured in much the same fashion as sediments. In cases where basalt recovery was fragmentary, individual continuous pieces were run through the magnetometer. Otherwise, whole sections of the basalt cores were run. Basalt cores were AF demagnetized at 15 mT only when anomalous inclinations indicated overprinting.

CARBON GEOCHEMISTRY

Shipboard carbon geochemistry analyses were conducted to monitor volatile hydrocarbons for safety considerations on a real-time basis and to characterize the initial content and type of organic matter in the sediments.

Hydrocarbon Gases

As required by safety considerations, concentrations of methane (C_1), ethane (C_2), and propane (C_3) hydrocarbons were monitored in the sediment cores at intervals of approximately 10 m. Headspace samples were obtained by removing a 5-cm^3 plug of sediment from the core as it arrived on deck with a No. 8 cork borer. The sample was placed immediately in a 21-ml glass vial that was sealed with a septum and metal crimp and then heated to 60°C for at least 45 min. The gas driven off was drawn into a syringe and analyzed.

The gas samples obtained were injected into a Hach-Carle AGC Series 100 Model 211 gas chromatograph equipped with a flame ionization detector and a 6-ft × 1/8-in. steel column packed with Porapak N:Q (80%/20%). Details of this method and the complete configuration of the gas chromatograph are given in the "Explanatory Notes" chapter for Leg 112 (Shipboard Scientific Party, 1988c).

Elemental Analysis

Sediments were analyzed on board ship for inorganic carbon and for total nitrogen, carbon, and sulfur.

Inorganic carbon was determined with a Coulometrics 5011 carbon dioxide coulometer equipped with a System 140 carbonate carbon analyzer. A known mass, ranging from 15 to 70 mg of dried and ground sediment, was reacted in a 2N HCl solution. The liberated CO_2 was titrated in a monoethanolamine solution with a colorimetric indicator, and the change in light transmittance was monitored with a photodetection cell. The percentage of carbonate was calculated from the inorganic carbon content assuming that all carbonate occurs as calcium carbonate:

$$CaCO_3 = IC \cdot 8.334.$$

Total nitrogen, carbon, and sulfur were determined using a N/C/S analyzer (Model NA 1500) from Carlo Erba Instruments. Mixtures of vanadium pentoxide and crushed samples were combusted in an oxygen atmosphere at 1000°C, converting organic and inorganic carbon to CO_2, sulfur to SO_2, and nitrogen to NO_2. The NO_2 was reduced to N_2 using copper. The gases were then separated by gas chromatography and measured with a thermal conductivity detector. Total organic carbon (TOC) was calculated from the difference between total carbon (TC) in the N/C/S analyzer and inorganic carbon (IC) in the coulometer:

$$TOC = TC - IC.$$

Rock-Eval Analysis

Organic matter type, thermal maturity, and hydrocarbon-producing potential were assessed with a Delsi, Inc., Rock-Eval II Plus T.O.C. instrument (Espitalie et al., 1977). Approximately 100 mg of dried and ground whole sediments were analyzed according to the standard procedures described in Emeis and Kvenvolden (1986).

INORGANIC GEOCHEMISTRY

Interstitial Water Sampling and Chemistry

For interstitial water sampling, 5- to 10-cm-long, whole-round sections were cut immediately after the cores arrived on deck, generally from the shallowest six cores and then from every third core thereafter. We sampled different holes at each site as needed to cover the entire depth range drilled at each site. Before squeezing, whole-round surfaces were carefully scraped with spatulas to remove potentially contaminated exteriors. Whole rounds were then placed into stainless steel squeezing devices (Manheim and Sayles, 1974) and squeezed with a hydraulic press. Interstitial water samples were filtered through 0.45-μm disposable filters and collected in plastic syringes.

Interstitial water samples were routinely analyzed for salinity as total dissolved solids with a Goldberg optical hand-held refractometer (Reichart); for pH and alkalinity by Gran titration with a Brinkmann pH electrode and a Metrohm autotitrator; for Cl, Ca, and Mg concentrations by titration; for SO_4 concentrations by ion chromatography with a Dionex 2120i chromatograph; and for Si, PO_4, and NH_4 concentrations by spectrophotometric methods with a Milton Roy Spectronic 1001 spectrophotometer using the analytical techniques described by Gieskes and Peretsman (1985). International Association of Physical Sciences Organizations (IAPSO) standard seawater was used for calibrating most techniques. The reproducibility of these techniques, expressed as 1 standard deviation of the means of multiple determinations of IAPSO standard seawater or of another standard, is as follows: alkalinity, 3%; Cl, 0.4%; Ca, <1%; Mg, 0.5%; SO_4, <2%; and Si, PO_4, and NH_4, 2%-3%.

We used flame spectrophotometric techniques with a Varian SpectrAA-20 atomic absorption unit to quantify concentrations of Na, K, Li, Sr, Rb, and Mn. Na and K were determined on 1/500 diluted aliquots by flame emission using an air-acetylene flame with Cs as an ionization suppressant. Li and Sr were determined on 1/6 diluted aliquots. Li was determined by emission using an air-acetylene flame, and Sr by atomic absorption using an air-acetylene flame with La as a realizing agent. Rb was determined directly on undiluted interstitial water samples by emission using an air-acetylene flame. Mn was determined by atomic absorption on 1/5 diluted aliquots with La added. Standards for all flame spectrophotometric techniques were matched in matrix composition to the samples. The reproducibility of these techniques, expressed as 1 standard deviation of the means of multiple determinations of IAPSO standard seawater or of another standard treated as samples, is as follows: Na, <1%-2%; K, <2%-3%; Li, <1%-2%; Rb, <1%-2%; Sr, <2%; and Mn, 2%-3%.

Chemical data for interstitial waters are reported in molar units in each site report.

IGNEOUS ROCKS

Core Curation and Shipboard Sampling

Igneous rocks were split into archive and working halves using a rock saw with a diamond blade. The petrologists decided on the orientation of each cut so as to preserve unique features and/or expose important structures. The archive half was described, and samples for shipboard and shore-based analyses were removed from the working half. Each piece was numbered sequentially from the top of each section, beginning with the number 1. Pieces that could be fitted together (like a jigsaw puzzle) were assigned the same number but were lettered consecutively (e.g., 1A, 1B, 1C, etc.).

Spacers were placed between pieces with different numbers but not between those with different letters and the same number. The presence of a spacer may represent a substantial interval of no recovery. Whenever the original unsplit piece was sufficiently large that the top and bottom could be distinguished before being removed from the core liner (i.e., the piece could not have rotated about a horizontal axis in the liner during drilling), a red wax cross was marked on the base of each piece.

Before the rock dried, sampling was conducted for shipboard physical properties, magnetics, X-ray diffraction (XRD), X-ray fluorescence (XRF), and thin-section studies. Minicores were taken from the working half and stored in seawater before measuring the physical properties. Nondestructive measurements of magnetic susceptibility and sometimes thermal conductivity were made on the archive half of the core. The archive half was then described in detail on the visual core description (VCD) form and photographed before storage.

Visual Core Descriptions

Hard rocks sampled from the basement were graphically represented on VCD forms specific to igneous and metamorphic rocks (see the VCD forms following the core barrel sheets). Copies of the VCD forms, as well as other prime data collected during Leg 130, are available on microfilm at all three ODP repositories. The left-hand column of the VCD (Fig. 9) is a graphical representation of the archive half. A horizontal line across the entire width of this column denotes a plastic spacer glued between rock pieces inside the liner. The number of each piece was also recorded, with oriented pieces indicated by the presence of an upward-pointing arrow to the right of the rele-

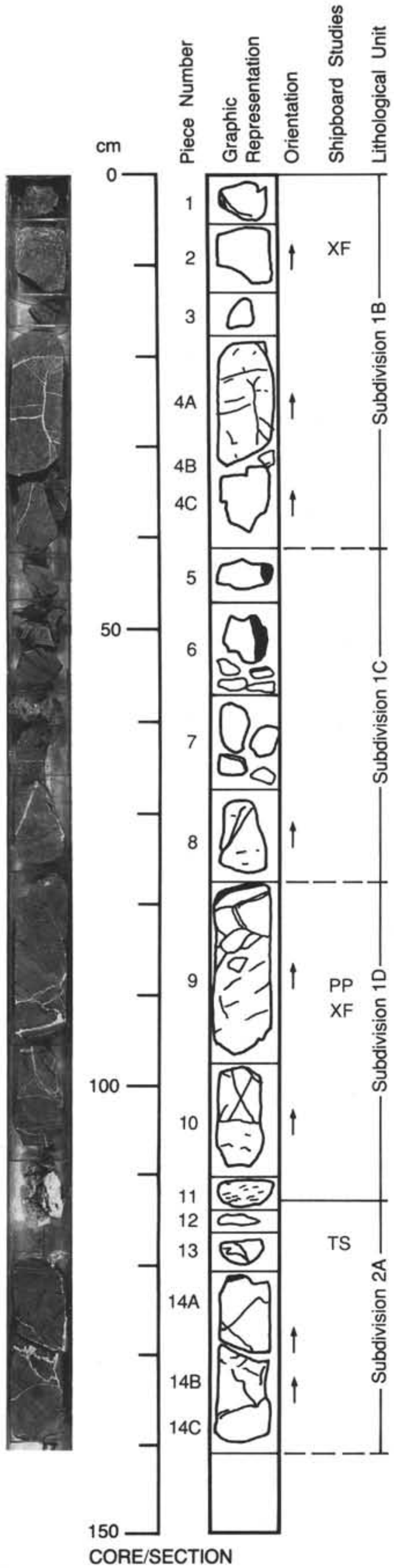

130-803D-69R-1

SUBDIVISION 1B: APHYRIC BASALT

Pieces 1-4

CONTACTS: None.
PHENOCRYSTS: Aphyric.
GROUNDMASS: Fine grained.
VESICLES: Nonvesicular.
COLOR: Gray to light-medium orange-brown.
STRUCTURE: Pillow.
ALTERATION: Highly altered, mottled appearance with light orange-brown patches.
VEINS/F RACTURES: <5%; 0.2-2 mm; subvertical and subhorizontal; calcite veins in Piece 4.

SUBDIVISION 1C: APHYRIC BASALT

Pieces 5-8

CONTACTS: Top of basalt pillow.
PHENOCRYSTS:
Pyroxene - <1%; ~1 mm; euhedral laths.
GROUNDMASS: Fine grained with glass rims.
VESICLES: Nonvesicular.
COLOR: Gray to dark gray, light-medium orange-brown, black glass rims.
STRUCTURE: Pillow.
ALTERATION: Moderately to highly altered with mottled and banded appearance.
VEINS/FRACTURES: <1-5%; <0.5-5 mm; irregular-subhorizontal; green mineral (celadonite?).

SUBDIVISION 1D: APHYRIC BASALT

Pieces 9, 10

CONTACTS: Margin of pillow.
PHENOCRYSTS: Aphyric.
GROUNDMASS: Fine grained with glassy rims.
VESICLES: Nonvesicular.
COLOR: Gray to dark gray, light-medium orange-brown, black glass rims.
STRUCTURE: Pillow.
ALTERATION: Moderately to highly altered.
VEINS/FRACTURES: <5%; <5 mm; subhorizontal; calcite-filled.

SUBDIVISION 2A: APHYRIC BASALT

Pieces 11-14

CONTACTS: Pieces 11-13 are a mixture of calcite and completely altered green basaltic glass (celadonite, serpentine, chlorite?). Probably the contact between pillow and limestone.
PHENOCRYSTS: Aphyric.
GROUNDMASS: Fine grained, glassy rim to top of Piece 14.
VESICLES: Nonvesicular.
COLOR: Medium gray-brown to light gray-brown/orange-brown.
STRUCTURE: Pillow.
ALTERATION: Very highly altered, mottled and banded appearance.
VEINS/FRACTURES: <5%; 0.5-5 mm; irregular; calcite.

Figure 9. Example of a completed VCD form for igneous rocks.

vant piece. Shipboard samples and studies were indicated in the "shipboard studies" column, using the following system of notation:

XD = X-ray diffraction analysis,
XF = X-ray fluorescence analysis,
PM = paleomagnetic measurements,
TS = thin-section billet, and
PP = physical properties measurement.

When the cores were described, checklists of macroscopic features were used to ensure consistent and complete descriptions, one for fine- and medium-grained extrusives and dikes, and another for plutonic rocks. The VCD form for fine- and medium-grained igneous rocks required the following information:

1. The leg, site, hole, core number and type, and section number.
2. A graphic representation of the core, including the rock piece numbers and positions of shipboard samples.
3. Lithologic unit boundaries, based on criteria such as the occurrence of glassy and quenched margins, trends of marked grain-size variation, and changes in petrographic type and phenocryst assemblages.

The following checklist was used for fine- and medium-grained igneous rocks. For each lithologic unit defined, the following were noted:

1. Unit number (consecutive downhole), including the numbers of the top and bottom pieces in the unit.
2. Rock name.
3. Contact type: glassy, intrusive, depositional, etc.
4. Phenocrysts: whether homogeneous or heterogeneous throughout the unit. For each phenocryst phase the following were given: abundance (%), average size (in millimeters), shape, degree of alteration (%), type and secondary phases, and any other comments.
5. Groundmass texture: glassy, microcrystalline, fine-grained (<1 mm), and medium-grained (1-5 mm). Any relative grain size changes within the unit from piece to piece were noted.
6. Color (dry).
7. Vesicles: size, shape, percentage, distribution, and nature of any fillings. Similar data for miaroles (vugs).
8. Structure: massive, pillowed, thin, or sheetlike, brecciated.
9. Alteration: type, form, distribution, and degree, ranging from fresh (<2% alteration present) to slightly altered (2%-10%), moderately altered (10%-40%), highly altered (40%-80%), very highly altered (80%-95%), and completely altered (95%-100%).
10. Veins/fractures: type, width, orientation, percentage present, and nature of infillings.

Finally, other comments were added, including continuity of the unit within the core and interrelationship between units. When the VCD form was complete and agreed upon by the igneous petrologists, the same information was then recorded in the VAX computer data-base HARVI. Each record was checked by the data-base program for consistency and printed in a format that could be pasted directly onto the final VCD record for subsequent curatorial handling.

Igneous rocks were classified mainly on the basis of mineralogy and texture. Basalts (fine-grained) and dolerites (medium-grained) were termed aphyric if phenocrysts were lacking or if they amounted to <1% of the rock. If porphyritic, the rock was designated as sparsely phyric (phenocryst content of 1%-2%), moderately phyric (2%-10%), or highly phyric (>10%). Estimates of phenocryst proportions were based on those visible with a hand lens or binocular microscope of about 10× power. Basaltic rocks were further classified by phenocryst type: a moderately plagioclase-olivine phyric basalt contains 2%-10% total phenocrysts, most of which are plagioclase with lesser amounts of olivine.

Thin-section Description

Thin-section billets of basaltic rocks recovered during Leg 130 were examined to help define subunit boundaries indicated on the VCDs and to confirm the identity of petrographic groups and/or alteration products. Petrographic descriptions, together with estimates of the various mineral phases (both primary and secondary), were made on the igneous thin-section description forms, which also were entered into the VAX computer data-base HRTHIN. Identification of secondary phases, such as clays and zeolites, was augmented in some cases by XRD.

X-ray Diffraction Analysis

A Philips ADP 3520 X-ray diffractometer was used for the XRD analysis of unknown, generally secondary, mineral phases. Instrument conditions were as follows: CuK-alpha radiation with Ni filter, 40 kV, 35 mA, goniometer scan from 2° to 50° 2θ, step size 0.02°, count time 2 s.

Samples were ground with water in an agate pestle and mortar until reduced to a very fine slurry. A suspension was then pipetted onto the surface of a glass slide and allowed to air dry before analysis. The resulting diffractograms were interpreted, in a few cases, with the aid of a computerized search-and-match routine using JCPDS powder files and tabulated data for clay minerals (Brindley and Brown, 1980).

X-ray Fluorescence Analysis

Samples from Site 803, considered to be either representative of individual lithologic subdivisions or possibly of unusual composition, were analyzed for major oxides and selected trace elements by XRF. The on-board XRF system is a fully automated, wave-length-dispersive, ARL 8420 spectrometer using a 3-kW rhodium X-ray tube as the excitation source for major and trace elements. Table 8 lists the elements analyzed as well as the operating conditions used.

Sample preparation involved (a) crushing the sample to a powder and (b) producing glass disks (for major element analysis) and pressed powder pellets (for trace element analysis). Initially, about 10 cm^3 of rock was removed from the core, and unwanted saw marks were erased by wet-grinding on a silicon carbide disk mill. Each sample was then ultrasonically washed in distilled water and methanol for 10 min and dried at 110°C for 2 hr. Larger pieces were reduced to <1-cm diameter by crushing them between two plastic disks in a hydraulic press. Powders were produced by grinding pieces in a motorized alumina mortar and pestle (to minimize contamination) for 10-30 min.

Major elements were determined on fused glass disks (Norrish and Hutton, 1969) to reduce matrix effects and variations in background. The disks are made by mixing 6 g of dry, lanthanum-doped (20% La_2O_3), lithium tetraborate flux (Spex #FF28-10) with 0.5 g of rock powder that has been ignited at about 1000°C in platinum-gold crucibles for 6-10 min and then poured into Pt-Au molds using a modified Claisse Fluxer apparatus. This 12:1 flux-to-sample ratio reduces matrix effects to the point where matrix corrections are unnecessary for normal basaltic to granitic compositions. Hence, the relationship between X-ray intensity and concentration becomes linear and can be described by:

$$C_i = (I_i \times m_i) - b_i,$$

Table 8. X-ray fluorescence analytical conditions, Leg 130.

Element	Detector	Collimator	Crystal	2θ	CT (s)
Fe	FC	F	LiF	57.52	40
Mn	KrC	F	LiF	62.98	40
Ti	FC	F	LiF	86.14	40
Ca	FC	C	LiF	113.16	40
K	FC	F	LiF	136.65	40
Si	FC	C	PET	109.25	40
Al	FC	C	PET	145.27	100
P	FC	C	Ge	140.94	200
Mg	FC	C	TlAP	44.87	200
Na	FC	C	TlAP	54.71	200
Nb	SC	F	LiF	21.37	200
Zr	SC	F	LiF	21.53	100
Y	SC	F	LiF	23.78	100
Sr	SC	F	LiF	25.13	100
Rb	SC	F	LiF	26.60	100
Zn	SC	F	LiF	41.79	60
Cu	SC	F	LiF	45.02	60
Ni	SC	C	LiF	48.67	60
Cr	FC	F	LiF	69.35	60
V	FC	F	LiF*	122.84	60

Notes: All elements measured on K-alpha line, using a rhodium X-ray tube operated at 60 kV and 50 mA. SC = NaI scintillation counter; FC = flow proportional counter (P10 gas); KrC = sealed krypton gas counter; F = fine and C = coarse; LiF = LiF (200) and LiF* = LiF (220); CT = counting time. Source: Shipboard Scientific Party, 1989b.

where

C_i = concentration of oxide i (wt%),
I_i = net peak X-ray intensity of oxide i,
m_i = slope of calibration curve for oxide i (wt%/cps), and
b_i = apparent background concentration for oxide i (wt%).

The slope m_i was calculated from a calibration curve derived from the measurement of well-analyzed reference rocks (BHVO-1, G-2, AGV-1, JGB-1, JP-1, Br, and DRN). The background b_i was determined on blanks or was derived by regression analysis from the calibration curves.

Trace elements were determined on pressed-powder pellets made by mixing 6 g of fresh rock powder with 1 g of wax. This mixture was then pressed into an aluminium cap with 7 tons of pressure. A minimum of 5 g of sample ensures the pellet will be "infinitely thick" for rhodium K-series radiation. For the computation of trace element concentrations from measured X-ray intensities, an off-line calculation program, based on routines from Bougault et al. (1977) and written by T. L. Grove and M. Loubet, was used.

SEDIMENTATION RATES

Sedimentation rate computations represent an important piece in the modern paleoceanographic puzzle because they add the element of time dimension to the lithostratigraphic column. We have chosen the time scales of Berggren et al. (1985a, 1985b), and Kent and Gradstein (1985) for the sedimentation rate method of transforming rock units into time units, as these scales are among the most complete syntheses available.

The correlation of biostratigraphic events to the geomagnetic polarity history is a key element in marine time scales; moreover, it is critically valuable in tropical regions where the rate of taxonomic evolution of sediment-forming marine microplankton has been greatest. A modest number of tropical deep-sea sediment sections are presently available that possess adequate magnetostratigraphies encompassing the past few million years. Thus, many Pliocene and Pleistocene biostratigraphic events are tied directly to the magnetic polarity zones in a low-latitude setting and, therefore, are considered to provide reasonably accurate biochronologies.

In contrast to this latest Neogene situation, it is perhaps surprising to note that we still do not possess a single continuous Miocene section with adequate magnetostratigraphy from a tropical/equatorial environment to refine biochronology in this interval. The compilation of Berggren et al. (1985b) of Miocene age estimates of the calcareous microfossil datums predominantly represents correlations in mid-latitude North and South Atlantic sections (e.g., DSDP Sites 516, 519, 521, 558, and 563). Recent ODP coring in the Indian Ocean, however, provided some insight into correlations of Miocene calcareous nannofossil biostratigraphy to magnetostratigraphy from an equatorial region, results that have been adopted here. Thus, it appears tenable to conclude that the established age estimates of many Miocene biostratigraphic events are associated with comparatively large uncertainties and, therefore, are poorly suited for establishing highly resolved sedimentation rate histories.

Shipboard biostratigraphy included information from two siliceous and two calcareous microfossil groups, implying that over 100 potential age-depth indicators were available for the Neogene. For a number of reasons, this wealth of information does not imply that we possess one control point every 0.25 m.y. over the past 25 Ma, but rather the existence of a fairly wide scatter of points in the age-depth graphs. This is so despite the fact that we have limited the uncertainties of the age-depth indications to depth (i.e., sample spacing) alone. It will be seen that the different microfossil groups commonly provide age discrepancies of about 1 m.y. for identical sample depths, discrepancies that are on the order of 10%–20% of the age of the sediment even in the late Miocene and Pliocene time interval. Such differences are considered to reflect problems largely associated with the assigned ages of the biostratigraphic events, implying that it is necessary to use selected age-depth indicators when estimating the sedimentation rate history.

The highly resolved, and fairly precise, Pliocene and Pleistocene biochronology allows a corresponding degree of detail to be included in the sedimentation rate estimates of these time intervals. In the Miocene, we have chiefly tried to recognize consistent linear scatters of age-depth indicators and, toward the extremes of these scatters, to select the marker events that describe a generalized, constant rate within the areas of scatter. For purposes of intersite comparison, it would be advantageous to rely on an identical set of biostratigraphic events when establishing sedimentation rates. This approach, therefore, will be adopted when permitted by the distribution of the critical age-depth points. An obvious consequence is that this procedure allows a fair amount of scatter of points around the proposed rate lines; this scatter reflects the biochronological uncertainty range at any given period of time for any given, or all, microfossil groups. Nevertheless, consistent offsets of points from the rate line then imply that the assigned age estimate of either the selected marker or the offset point needs revision.

Until the day when we possess a more accurate Miocene biochronology, which can be created only through the retrieval and direct correlation of adequate magnetostratigraphies, it will remain difficult to improve the resolution of Miocene sedimentation rate histories. It follows (1) that the low-resolution sedimentation rate records presented here make it possible to decipher the general pattern of change, but hardly to view the entire chain of details making up the pattern; and (2), that we still cannot properly assess the rates of many of the important processes that characterized the development of the Miocene deep-sea environment.

All of the available biostratigraphic information from each hole cored during Leg 130 has been listed in table format and portrayed graphically as age-depth plots. Clusters of points in some sections are shown at enlarged scales to help identify individual points. Those graphs with enlarged scales of holes have grids in contrast to the graphs with the complete hole information. To emphasize the sedimentation rate variability through time, sedimentation rates were plotted vs. age for one or several holes at each site. That variability depended entirely on the selected control points indicating rate changes, and hence involved subjective bias.

All sedimentation rates were calculated using mid-points in the observed depth uncertainty range, and rates between control points were obtained through linear interpolation.

PHYSICAL PROPERTIES

Shipboard measurements of physical properties provided information that aids characterization of lithologic units, correlation of lithology with downhole geophysical logging results, and interpretation of seismic reflection and other geophysical data. The goal of the physical properties program of Leg 130, in addition to providing a link between lithologic and geophysical data, was to identify the physical signals in the sediments that result from carbonate dissolution and diagenesis.

Several types of measurements were performed on the whole-round core sections. Measurements of bulk density, compressional wave velocity, and magnetic susceptibility were provided by the multisensor track (MST). The MST incorporated a gamma-ray attenuation porosity evaluator (GRAPE), a compressional wave (*P*-wave) core logger (PWL), and a magnetic susceptibility monitor. Thermal conductivity measurements with the needle probe method were performed at discrete intervals in whole-round sections of soft sediments.

Physical properties measurements made on samples obtained from the split cores included vane shear strength, electrical resistivity, compressional wave velocity and attenuation, and index properties. Samples were chosen to be representative of the core or section in undisturbed sediment. Measurements and samples were obtained generally at a frequency of two per section in the oozes, one per section deeper in the hole.

Multisensor Track

The MST incorporated the GRAPE, *P*-wave logger, and magnetic susceptibility devices in scans of the whole-round core sections. Individual unsplit core sections were placed horizontally on the MST, which moved the section through the three sets of sensors.

The GRAPE measured average bulk density over 1-cm intervals by comparing the attenuation of gamma rays through the cores with attenuation through an aluminum standard (Boyce, 1976). The GRAPE data were most reliable in the APC cores. The drilling slurry between the core and liner and between the XCB "biscuits" yielded lower bulk densities, and thus GRAPE data from the XCB cores could be used only as an indication of trends and highs in bulk densities. GRAPE data were useful in correlating between holes and sites by observing peak-to-peak spacings and general trends in the data.

Wet-bulk density was also determined by means of the GRAPE special 2-min count technique, as described by Boyce (1976). The GRAPE measurements were made perpendicular to bedding on half-round samples cut from the cores using the double-bladed saw. All counts for the samples and accompanying air (background) counts were made in duplicate and averaged. Grain density values from gravimetric measurements were used to correct the wet-bulk density determined by the GRAPE for deviation of the grain density of the sample from that of quartz. The precision estimated for this technique is $\pm 1.5\%$ (Boyce, 1976).

The PWL transmitted a 500-kHz compressional wave pulse through the core at a repetition rate of 1 kHz. The transmitting and receiving transducers were aligned perpendicular to the core axis. A pair of displacement transducers monitored the separation between the compressional wave transducers; therefore, variations in the outside diameter of the liner did not degrade the accuracy of the velocities. Measurements were taken at 2-cm intervals. Generally, only the APC cores were measured, as the XCB and RCB cores had voids between the core and the liner that caused transmission losses. Weak returns with signal strengths below a threshold value of 100 were removed.

The MST magnetic susceptibility procedures are included in the "Paleomagnetics" section of this chapter (this volume).

Thermal Conductivity

Thermal conductivity measurement techniques used during Leg 130 have been described by Von Herzen and Maxwell (1959) and Vacquier (1985). Measurements were made with a Woods Hole Thermcon-85 unit, and all data are reported in units of $W/m \cdot K$. The estimated error in the measurements is about 5%–10%. Data were not corrected for *in-situ* pressure and temperature.

To reduce background thermal transients, cores were allowed to equilibrate in their liners until the sediments reached a stable temperature. Needle probes were inserted in sections 2, 3, 4, and 5 of every soft sediment section through holes drilled through the liners. Sample temperatures were monitored with the thermistors in the probes, without applying a current to the heater wires. The actual test sequence was started once the background temperature drift was reduced to 0.04°C/min. Thermal conductivity was calculated from the rate of temperature rise in the probe while a heater current was flowing. The temperature rise in the probe varies logarithmically with time as:

$$T(t) = (q/4\pi k)\ln(t) + \text{const.},$$

where k is the thermal conductivity, T and t are temperature and time, respectively, and q is the heat generated per unit length of the probe. From this equation, we can derive thermal conductivity from the slope of temperature vs. the logarithm of time.

Measurements of thermal conductivity were performed until the sediment became too lithified to insert the needle probes. Unfortunately, many problems were encountered when using the probes, and no spares were available. One of the probes malfunctioned while measuring cores from Site 803, allowing only three sections to be measured per core. Another probe yielded data with high drift, so the number of sections measured per core was decreased when we measured the cores from Site 806. Thermal conductivity was not measured in Site 807 cores. Analyses of data from the first site showed considerable scatter in the data, even within individual cores. This is probably related to the problem with the probe calibrations, but no time was available to correct for this. The data given are the mean values calculated for each core; thus, only one value per core is given.

Electrical Resistivity

The Wayne-Kerr precision component analyzer was used to measure resistivity, following the procedures outlined in the "Explanatory Notes" chapter of Leg 127 (Shipboard Scientific Party, 1990b). We measured the electrical resistivity of the sediments once per section using a four-electrode configuration, which consists of four 2-mm stainless steel rods with an electrode spacing of 13 mm. A 20-kHz square wave current was applied to the outer electrodes, and the difference in potential between the two inner electrodes was measured. The size of the current (typically 50 mA) was measured over a resistor in the outer circuit.

The electrodes were buried approximately 1 cm into the split-core surface after measuring the resistance of seawater in another split liner, thus avoiding geometric differences between sediment and water samples. Measurements were made in two directions (horizontal and vertical). Unfortunately, erroneous readings of resistance began during the measurement of cores from Site 803. This problem was probably caused by epoxy leaking into the assembly in which the probes were embedded. Unfortunately, there was no time to repair the probe assembly. Analyses of the data before this malfunction showed a great deal of scatter, apparently the result of different measurement techniques used by different workers. In light of these problems, and because good resistivity logs were obtained at Site 803, the laboratory electrical resistivity program was suspended for the duration of Leg 130.

Vane Shear Strength

The undrained shear strength of the sediment was determined with the ODP motorized miniature vane shear device following the procedures of Boyce (1976). The vane rotation rate was set to 60°/min. The vane used for all measurements had a 1:1 blade ratio with a dimension of 1.27 cm.

The vane shear device measured the torque and strain at the vane shaft with a torque transducer and potentiometer, respectively. Output for torque and strain was recorded on a Hewlett-Packard XY recorder in volts. The shear strength reported was the peak strength determined from the torque vs. the strain plot, as detailed in the "Explanatory Notes" chapter of Leg 110 (Shipboard Scientific Party, 1988b). In addition to the peak shear strength, residual strength was determined from the same plot when the failure was not dominated by cracking of the sample (Pyle, 1984).

When we analyzed the vane tests, we assumed that a cylinder of sediment was uniformly sheared about the axis of the vane in an undrained condition, with cohesion as the principal contributor to shear strength. Departures from this assumption included progressive cracking within and outside of the failing specimen, uplift of the failing core cylinder, drainage of local pore pressures (i.e., the test can no longer be considered as undrained), and stick-slip behavior. Also, silts and sands provided increased friction effects. Because the sediments cored during Leg 130 were predominantly silt-, sandy silt-, or clayey silt-sized, friction effects and sample draining during testing were likely. The rate of rotation was increased to that recommended by Boyce (1976) to allow a faster test, which we hoped would minimize the problem of draining. In light of these problems, and because of the expected disturbance during drilling, the minivane test cannot be considered a measure of the true shear strength of the sediment. In a laboratory situation, only properly controlled or simple shear tests can be used to provide adequate *in-situ* strength. The minivane test does, however, provide an estimate of strength and a means of comparing downcore and between-hole parameters.

Compressional Wave Velocity

We obtained compressional *P*-wave velocity measurements by means of two different systems during Leg 130, depending on the degree of lithification of the sediment. *P*-wave velocities were measured in unconsolidated sediment using a Dalhousie University/Bedford Institute of Oceanography Digital Sound Velocimeter (DSV; Mayer et al., 1987). The system used on Leg 130 was provided by the Departmente de Geologie Dynamique, Université de Paris VI, and funded by CNRS, France. Velocity calculations were based on the accurate measurement of the time of flight of an impulsive acoustic signal traveling between a pair of piezoelectric transducers inserted in the split sediment cores. The signal used was a 2-μs square wave; the transducers have resonances at about 250 and 750 kHz. A dedicated microcomputer controlled all functions of the velocimeter. The transmitted and received signals were digitized by a Nicolet 320 digital oscilloscope and transferred to the microcomputer for processing. The DSV software selected the first arrival and calculated sediment velocity; the full waveform was stored for later calculation of attenuation.

Four transducers were used; two of them, separated by approximately 7 cm, measured the vertical (along the core axis) *P*-wave velocity, and the other two, separated by approximately 3.5 cm, measured the horizontal (parallel to bedding) velocity. The transducers were firmly fixed at one end on a steel plate so that their separation would not change during velocity determinations. Thermistors in the transducer probes monitored temperatures while measurements were being taken.

Periodically, the separation was precisely evaluated by running a calibration procedure in distilled water. A value of sound velocity in distilled water was determined (based on standard equations) for the measured temperature, with the computer calculating the transducer separation using the signal traveltime. At each sampling interval (usually two per section), the transducers were carefully inserted into the split section and velocity was measured in both directions.

The Hamilton Frame velocimeter was used to measure compressional wave velocities at 500 kHz in discrete sediment samples when induration made it difficult to insert the DSV transducers without making any perturbations around them and in lithified sediments and basement rocks when insertion became impossible. Samples were carefully cut using a double-bladed diamond saw to obtain parallel faces. Sample thickness was measured directly from the velocimeter-frame lead screw. Zero traveltimes for the velocity transducers were estimated by linear regression of traveltime vs. distance for a series of aluminum and lucite standards. Filtered seawater was used to improve the acoustic contact between the sample and the transducers. The DSV oscilloscope and processing software was used to digitize waveforms, calculate velocities, and store the waveforms for later attenuation calculations.

Measurements were performed after the cores had equilibrated to room temperature (approximately 3 hr). Thus, *P*-wave velocity data are given at laboratory conditions (1 atm., 26°C approximately).

Index Properties

Index properties (bulk density, grain density, water content, porosity, and dry density) were calculated from measurements of wet and dry weights and dry volume. Samples of approximately 10 cm^3 were taken to determine the index properties. Soft sediment samples were placed in precalibrated aluminum containers before being measured for weight and volume. Index properties measurements for lithified sediment and basement rock samples were made on crushed portions of the sample cubes cut for velocity determinations.

Sample weights were determined aboard ship to a precision of ± 0.01 g using a Scitech electronic balance. Volumes were determined using a Quantachrome Penta-Pycnometer, a helium-displacement pycnometer. The Quantachrome pycnometer measured volumes to an approximate precision of 10^{-4} cm^3.

It has been observed that the frequent air pressure drops in the lab stack affect the performance of the pycnometer. Another problem in the consistency of the pycnometer arises as a result of slightly different pressures measured during different calibration runs. The variability associated with pressure drops was minimized by repeating the measurements until two volumes for the same cell agreed to within 0.05 cm^3. To correct for the differences associated with changes in calibration pressure, a standard was included in every other pycnometer run. The standard was rotated through each of the cells so that changes in the cells could be monitored. The sample volumes were then corrected by the difference between the measured standard volume and the known standard volume.

The entire set of beakers was painstakenly calibrated during transit to the first site. This recalibration was conducted by calculating the densities of the beakers, using weights and volumes already present in the data base. Because the beakers are made of aluminum, their densities should be near 2.7 g/cm^3. However, many of the calculated densities were off by 0.1 g/cm^3 or more. Thus, the beakers were all weighed and run through the pycnometer, and the densities recalculated. These values were entered into the "physprops" data base.

At Site 803, wet and dry volumes were measured for each sample. It quickly became apparent that the samples from subsequent sites could only be run once through the pycnometer if we were to keep up with the desired sampling frequency. Examination of the data indicated that the dry volumes measured by the pycnometer are more accurate than the wet volumes, because of the presence of volatiles in the wet samples that apparently result in erroneous pressure readings. Therefore, for subsequent sites, only dry samples were run through the pycnometer. Dry weight and volume measurements were obtained after the samples were oven dried at 110°C for 24 hr and allowed to cool in a desiccator. A salt correction, assuming 35-ppt interstitial fluid salinity, was applied to density and porosity computations as per Hamilton (1971).

Wet-bulk density was calculated from the wet and dry weights (W_w and W_d, respectively) and dry volumes (V_d). The wet volume (V_w), used to calculate bulk density, was calculate by adding the weight of the water lost through drying of the sample to the dry volume, using the following equation:

$$V_w = V_d + (W_w - W_d)/\delta_f,$$

where δ_f is the density of evaporated water and is assumed to be equal to 1. The dry volume, V_d, includes both the volume of the sediment or rock constituents and the volume of salt remaining in the sample upon drying. Then, wet-bulk density was calculated in the normal manner as follows:

$$\delta_{bw} = W_w/V_w.$$

Porosity, water content (calculated as a percentage of dry weight), grain density, and dry-bulk density were also calculated using the calculated wet volume, according to the equations of Boyce (1976).

DOWNHOLE MEASUREMENTS

General

Downhole logs can be used to characterize the geophysical, geochemical, and structural properties of a drilled sequence. Log measurements have a distinct advantage over core-based measurements in that they represent continuous and *in-situ* measurements of the borehole. After coring is completed in a particular hole, a combination of sensors is lowered downhole on a seven-conductor cable, and each of several measuring devices continuously monitors properties of the adjacent formation. Under rough sea conditions, a wireline heave compensator can be used to minimize the effects of ship heave on the tool position in the borehole. The depths of investigation are sensor-dependent, and data are typically recorded at 15-cm intervals.

Three different tool strings of Schlumberger sensors were used on Leg 130: (1) a "geophysical" tool string, (2) a "geochemical" tool string, and (3) the formation microscanner (FMS). The Lamont-Doherty temperature tool was also attached at the base of each tool string to obtain heat-flow information.

The Geophysical Tool String

The geophysical tool string typically consists of the natural gamma-ray spectrometry tool (NGT), the phasor dual-induction tool (DITE), the long-spacing digital sonic velocity tool (LSS), and the lithodensity tool (HLDT). At Hole 803D, because of tool failures, a borehole-compensated sonic velocity tool (BHC) was also used. The geophysical tool string is designed to measure the sonic-wave propagation properties of the borehole through measurements in the formation of the compressional wave velocity; the deep, intermediate, and shallow resistivity; and the formation density. The sonic velocity data, when combined with the information on density, are used to calculate an impedance log and generate a synthetic seismogram for the logged sequence. The natural gamma radiation tool is run on each combination tool string to provide a common basis for log correlations.

The dual induction tool (DITE) provides three different measurements of electrical resistivity, each with a different radial depth of investigation. Two induction devices ("deep" and "medium" resistivity) send high-frequency alternating currents through transmitter coils, creating magnetic fields that induce secondary (Foucalt) currents in the formation. These ground-loop currents produce new inductive signals, proportional to the conductivity of the formation, that are recorded by a series of receiving coils. The measured conductivities are converted to resistivity. A third device (the "spherically focused" resistivity [SFR] tool) measures the current necessary to maintain a constant voltage drop across a fixed interval. The vertical resolution is on the order of 2 m for the two induction devices and about 1 m for the SFR. The data can be corrected for irregularities in borehole diameter.

In general, resistivity responds to the inverse square root of porosity (Archie, 1942). Water salinity, clay content, hydrocarbon content, and temperature are also important factors in controlling the electrical resistivity of rocks. Other factors that may influence the resistivity of a rock include the concentration of hydrous and metallic minerals, formation vesicularity, and the geometry of the interconnected pore space.

The long-spacing digital sonic tool (LSS) uses two acoustic transmitters and two receivers to measure the time required for sound waves to travel along the borehole wall over source-receiver distances of 8, 10, and 12 ft (2.4, 3.0, and 3.6 m). First arrivals for the individual source-receiver paths are used to calculate the velocities of the waves traveling in the formation; the tool measures four traveltimes at each measurement depth as there are four possible paths. The borehole-compensated sonic tool (BHC; also known as the short spacing sonic tool) has two sources and two receivers configured to provide four symmetric and redundant measurements of acoustic traveltime. The source-receiving spacing on this tool provides two 3-ft- and two 5-ft-interval transit time measurements. In poor hole conditions, such as are often experienced by ODP, the LSS provides more reliable data than the BHC. Only compressional wave velocities are determined aboard the ship, but full sonic waveforms are recorded for post-cruise processing to determine shear wave and Stonely wave velocities. The vertical resolution of the LSS and the BHC is about 2 ft (0.61 m). Logs can be corrected for cycle skipping (misidentified arrivals) because of the four-way measurement redundancy. Compressional wave velocity is dominantly controlled by porosity and lithification; decreases in porosity and increases in lithification typically cause velocity to increase with depth in a sedimentary sequence.

The lithodensity tool (HLDT) uses a 0.66 MeV ^{137}Ce gamma-ray source for its density measurements. The source is mounted in the tool body and a caliper arm presses it and a pair of detectors against the borehole wall. The density measurement is based upon Compton scattering of the gamma rays within the formation and, thus, actually is a measurement of electron density. Because most rock-forming elements have atomic weights that are twice their atomic numbers, the electron density can be converted directly to bulk density. In addition, the tool also records a photoelectric effect index. Photoelectric absorption occurs in the energy window below 150 KeV and depends upon the energy of the incident gamma ray, the atomic cross section, and the nature of the atom. The measurement is almost independent of porosity and can therefore be used directly as a matrix lithology indicator. The density and photoelectric effect measurements require excellent contact with the borehole wall; the tool provides a measure of this and corrections can be made for excessive borehole roughness. The vertical resolution of the measurement is about 0.3 m.

The Geochemical Tool String

The geochemical tool string used on Leg 130 consists of a natural gamma-ray tool (NGT), an induced gamma-ray spectroscopy tool (GST), and the aluminum clay tool (ACT). Relative concentrations of Si, Ca, Fe, S, H, and Cl can be derived on shipboard, as well as weight percent abundance of K, U, Th, and Al. Further shore-based processing can produce abundance logs of the first six elements mentioned plus Gd and Ti.

The NGT measures the natural radioactivity of the formation. Most gamma rays are emitted by the naturally occurring radioactive isotope ^{40}K and by a series of U and Th isotopes and their daughters. The gamma radiation originating in the formation close to the borehole wall is measured by a sodium iodide scintillation detector mounted inside the sonde. The energy spectrum measured by the sodium iodide detector is divided into five discrete energy windows. The total counts recorded in each window, for a specified depth in the well, are processed at the surface to give elemental abundances of K, U, and Th. The tool has a depth of investigation of about 0.3–0.5 m. The NGT data are also corrected for borehole diameter variations. The tool is run on every combination tool string to serve as a basis for depth correlations between separate runs.

The elements K, U, and Th tend to be most abundant in clay minerals, and consequently the gamma-ray curve is commonly used to estimate the sediment clay content. Uranium tends to be concentrated in organic-rich sediments because of its redox chemistry (Fertl, 1983) and can be an indirect indicator of sapropelic layers. However, silicic volcaniclastics and potassium-feldspar-rich sandstones also can have high abundances of these three elements.

The GST consists of a pulsed 14-MeV neutron generator and a gamma-ray scintillation detector. The incident neutrons lose energy through inelastic scattering in the formation and eventually are captured by elemental nuclei when they reach thermal energy levels (about 0.02 eV). After capture, gamma rays are emitted; these gamma rays are detected by the tool. The 256-channel energy spectrum is deconvoluted to determine the relative abundance of Ca, Si, Fe, Cl, H, and S on board the ship. The raw logs were extensively reprocessed post-cruise by the Borehole Research Group at Lamont-Doherty Geological Observatory to produce percentage data for these elements as well as Gd and Ti. Because the depth being investigated is shallow, the logs also had to be corrected for variability in borehole diameter.

Aluminum abundance is measured by the ACT, which uses a different form of neutron activation analysis than the GST. When aluminum absorbs a neutron from the 2.5-MeV ^{252}Cf source, it forms an unstable nucleus with a half-life of about 2 min. When it decays, a characteristic gamma ray is emitted within the energy windows of the natural gamma tool. The contribution to the gamma-ray spectrum caused by natural radiation is removed by running NGT tools both above and below the neutron source; the detector above measures the natural radiation before activation, and the detector below measures the induced radiation.

The Formation Microscanner

The formation microscanner (FMS) produces high-resolution images of the microresistivity character of the borehole wall that can be used for detailed sedimentological or structural interpretations (Ekstrom et al., 1986; Pezard and Luthi, 1988). Schlumberger originally introduced the tool in 1986, but it was not suitable for use in the narrow-gauge drill pipe used by the ODP. A modified sensor was consequently developed by Schlumberger and first deployed during Leg 126.

The FMS tool consists of 16 electrode "buttons" on each of four orthogonal pads that are pressed against the borehole wall. The electrodes are spaced about 2.5 mm apart and are arranged in two diagonally offset rows of eight electrodes each. Shore-based processing corrects the offset rows to one level, which doubles the horizontal resolution to about 1.25 mm. The FMS tool string contains a general purpose inclinometry tool (GPIT) that spatially orients the resistivity measurements through the use of an accelerometer and from the declination and inclination of the Earth's magnetic field vector. The raw data undergo extensive processing to transform the individual microresistivity traces into complete, spatially oriented images. Because of limited shipboard capabilities for processing on Leg 130, only limited reprocessing was carried out at sea.

Possible applications of the FMS-derived images include (1) making detailed correlations between coring and logging depths; (2) finding the orientation of cores; (3) mapping fractures, faults, foliations, and formation structures; and (4) determining strikes and dips of bedding. The FMS can also be used to measure stress in the borehole. The FMS provides precise measurements of borehole diameter in two orthogonal directions. In an isotropic, linearly elastic rock subjected to an anisotropic stress field, breakouts form along the borehole wall as a result of compressive stress concentrations exceeding the strength of the rock. Under these conditions, the breakout orientation develops in the direction of the least principal horizontal stress. It has been demonstrated previously that stress orientations deduced from rock breakouts are consistent with other independent stress indicators (Bell and Gough, 1979; Zoback et al., 1988).

REFERENCES

Archie, G. E., 1942. The electrical resistivity log as an aid in determining some reservoir characteristics. *J. Petrol. Tech.*, 5:1–8.

Aubry, M.-P., Berggren, W. A., Kent, D. V., Flynn, J. J., Klitgord, K. D., Obradovich, J. D., and Prothero, D. R., 1988. Paleogene geochronology: an integrated approach. *Paleoceanography,* 3:707–742.

Backman, J., 1986. Late Paleocene to middle Eocene calcareous nannofossil biostratigraphy from the Shatsky Rise, Walvis Ridge and Italy. *Palaeogeogr., Palaeoclimatol., Palaeoecol.,* 57:43–59.

———, 1987. Quantitative calcareous nannofossil biochronology of middle Eocene through early Oligocene sediment from DSDP Sites 522 and 523. *Abh. Geol. Bundesanst. Austria,* 39:21–31.

Backman, J., and Pestiaux, P., 1986. Pliocene *Discoaster* abundance variations, Deep Sea Drilling Project Site 606: biochronology and paleoenvironmental implications. *In* Ruddiman, W. F., Kidd, R. B., Thomas, E., et al., *Init. Repts. DSDP,* 94, Pt. 2: Washington (U.S. Govt. Printing Office), 903–910.

Backman, J., and Shackleton, N. J., 1983. Quantitative biochronology of Pliocene and early Pleistocene calcareous nannofossils from the Atlantic, Indian and Pacific oceans. *Mar. Micropaleontol.,* 8:141–170.

Backman, J., Schneider, D. A., Rio, D., and Okada, H., 1990. Neogene low-latitude magnetostratigraphy from Site 710 and revised age estimates of Miocene nannofossil datum events. *In* Duncan, R. A., Backman, J., Peterson, L. C., et al., *Proc. ODP, Sci. Results,* 115: College Station, TX (Ocean Drilling Program), 217–276.

Baldauf, J. G., 1985. A high resolution late Miocene-Pliocene diatom biostratigraphy for the eastern equatorial Pacific. *In* Mayer, L., Theyer, F., Thomas, E., et al., *Init. Repts. DSDP,* 85: Washington (U.S. Govt. Printing Office), 457–475.

Barron, J. A., 1985a. Late Eocene to Holocene diatom biostratigraphy of the equatorial Pacific Ocean, Deep Sea Drilling Project Leg 85. *In* Mayer, L., Theyer, F., Thomas, E., et al., *Init. Repts. DSDP,* 85: Washington (U.S. Govt. Printing Office), 413–447.

________, 1985b. Miocene to Holocene planktic diatoms. *In* Bolli, H. M., Saunders, J. B., and Perch-Nielsen, K. (Eds.), *Plankton Stratigraphy:* Cambridge (Cambridge Univ. Press), 763–809.

________, 1989. The late Cenozoic stratigraphic record and hiatuses of the northeast Pacific: results from the Deep Sea Drilling Project. *In* Winterer, E. L., Hussong, D. M., and Decker, R. W. (Eds.), *The Eastern Pacific Ocean and Hawaii* (Vol. N): Boulder, CO (Geol. Soc. Am.), 311–322.

Barron, J. A., Keller, G., and Dunn, D. A., 1985a. A multiple microfossil biochronology for the Miocene. *In* Kennett, J. P. (Ed.), *The Miocene Ocean: Paleoceanography and Biogeography.* Mem. Geol. Soc. Am., 163:21–36.

Barron, J. A., Nigrini, C. A., Pujos, A., Saito, T., Theyer, F., Thomas, E., and Weinreich, N., 1985b. Synthesis of biostratigraphy, central equatorial Pacific, Deep Sea Drilling Project Leg 85: refinement of Oligocene to Quaternary biochronology. *In* Mayer, L., Theyer, F., Thomas, E., et al., *Init. Repts. DSDP,* 85: Washington (U.S. Govt. Printing Office), 905–934.

Bell, J. S., and Gough, D. I., 1979. Northeast-southwest compressive stress in Alberta: evidence from oil wells. *Earth Planet. Sci. Lett.,* 45:475–482.

Berggren, W. A., 1969. Rates of evolution in some Cenozoic planktonic foraminifera. *Micropaleontology,* 15(3):351–365.

Berggren, W. A., Kent, D. V., and Flynn, J. J., 1985a. Jurassic to Paleogene: Part 2. Paleogene geochronology and chronostratigraphy. *In* Snelling, N. J. (Ed.), *The Chronology of the Geological Record.* Mem. Geol. Soc. (London), 10:141–195.

Berggren, W. A., Kent, D. V., Flynn, J. J., and Van Couvering, J. A., 1985b. Cenozoic geochronology. *Geol. Soc. Am. Bull.,* 96:1407–1418.

Berggren, W. A., Kent, D. V., and Van Couvering, J. A., 1985c. The Neogene: Part 2. Neogene geochronology and chronostratigraphy. *In* Snelling, N. J. (Ed.), *The Chronology of the Geological Record.* Mem. Geol. Soc. (London), 10:211–260.

Berggren, W. A., and Miller, K. G., 1988. Paleogene tropical planktonic foraminiferal biostratigraphy and magnetobiochronology. *Micropaleontology,* 34(4):362–380.

Blow, W. H., 1969. Late middle Eocene to Recent planktonic foraminiferal biostratigraphy. *In* Brönniman, P., and Renz, H. H., (Eds.), *Proceedings of the First International Conference on Planktonic Microfossils, Geneva:* Leiden (E. J. Brill), 1:199–422.

________, 1979. *The Cainozoic Globigerinida:* Leiden (E. J. Brill).

Bolli, H. M., and Premoli-Silva, I., 1973. Oligocene to Recent planktonic foraminifera and stratigraphy of the Leg 15 sites in the Caribbean Sea. *In* Edgar, N. T., Saunders, J. B., et al., *Init. Repts. DSDP,* 15: Washington (U.S. Govt. Printing Office), 475–497.

Bolli, H. M., and Saunders, J. B., 1985. Oligocene to Holocene low latitude planktonic foraminifera. *In* Bolli, H. M., Saunders, J. B., and Perch-Nielsen, K. (Eds.), *Plankton Stratigraphy:* Cambridge (Cambridge Univ. Press), 155–262.

Bougault, H., Cambon, P., and Toulhoat, H., 1977. X-ray spectrometric analysis of trace elements in rocks: correction for instrumental interferences. *X-Ray Spectrom.,* 6:66–72.

Boyce, R. E., 1976. Definitions and laboratory techniques of compressional sound velocity parameters and wet-water content, wet-bulk density, and porosity parameters by gravimetric and gamma ray attenuation techniques. *In* Schlanger, S. O., Jackson, E. D., et al., *Init. Repts. DSDP,* 33: Washington (U.S. Govt. Printing Office), 931–958.

Brindley, G. W., and Brown, G. (Eds.), 1980. *Crystal Structures of Clay Minerals and Their X-ray Identification.* Mineral. Soc. Monogr., No. 5.

Burckle, L. H., 1972. Late Cenozoic planktonic diatom zones from the eastern equatorial Pacific. *Nova Hedwigia Beih.,* 39:217–246.

Burke, S. C., 1981. Recent benthic foraminifera of the Ontong Java Plateau. *J. Foraminiferal Res.,* 11:1–19.

Caron, M., 1985. Cretaceous planktonic foraminifera. *In* Bolli, H. M., Saunders, J. B., and Perch-Nielsen, K. (Eds.), *Plankton Stratigraphy:* Cambridge (Cambridge Univ. Press), 17–86.

Douglas, R., 1973. Benthic foraminiferal biostratigraphy in the central North Pacific, Leg 17, Deep Sea Drilling Project. *In* Winterer, E., Ewing, J., et al., *Init. Repts. DSDP,* 17: Washington (U.S. Govt. Printing Office), 607–672.

Dunham, R., 1962. Classification of carbonate rocks according to depositional texture. *In* Ham, W. E. (Ed.), *Classification of Carbonate Rocks:* Tulsa, OK (AAPG), 108–121.

Ekstrom, M. P., Dahan, C. A., Chen, M.-Y., Lloyd, P. M., and Rossi, D. J., 1986. Formation imaging with microelectrical scanning arrays. *Trans. SPWLA Annu. Logging Symp.,* 27th, Paper BB.

Emeis, K.-C., and Kvenvolden, K. A., 1986. Shipboard organic geochemistry on *JOIDES Resolution. ODP Tech. Note,* No. 7.

Espitalié, J., Laporte, J. L., Madec, M., Marquis, F., Leplat, P., Paulet, J., and Boutfeu, A., 1977. Method rapide de caracterisation des roches mère de leur potentiel petrolier et de leur degree d'evolution. *Rev. Inst. Fr. Pet.,* 32:23–42.

Fenner, J., 1984. Eocene-Oligocene planktic diatom stratigraphy in the low latitudes and high southern latitudes. *Micropaleontology,* 30: 319–342.

________, 1985. Late Cretaceous to Oligocene planktic diatoms. *In* Bolli, H. M., Saunders, J. B., and Perch-Nielsen, K. (Eds.), *Plankton Stratigraphy:* Cambridge (Cambridge Univ. Press), 713–762.

Fertl, W. H., 1983. Gamma ray spectral logging: a new evaluation frontier. *World Oil,* 197:99–112.

Fisher, R. V., and Schmincke, H.-U., 1984. *Pyroclastic Rocks:* Berlin-Heidelberg-New York (Springer-Verlag).

Fornaciari, E., Raffi, I., Rio, D., Villa, G., Backman, J., and Olafsson, G., 1990. Quantitative distribution patterns of Oligocene and Miocene calcareous nannofossils from western equatorial Indian Ocean. *In* Duncan, R. A., Backman, J., Peterson, L. C., et al., *Proc. ODP, Sci. Results,* 115: College Station, TX (Ocean Drilling Program), 237–254.

Gieskes, J. M., and Peretsman, G., 1985. Water chemistry procedures aboard *JOIDES Resolution*—some comments. *ODP Tech. Note,* No. 5.

Hamilton, E. L., 1971. Prediction of *in-situ* acoustic and elastic properties of marine sediments. *Geophysics,* 36:266–284.

Hermelin, J.O.R., 1989. Pliocene benthic foraminifera from the Ontong-Java Plateau (western equatorial Pacific Ocean): faunal response to changing paleoenvironment. *Spec. Publ., Cushman Found. Foraminiferal Res.,* 26:1–143.

Kennett, J. P., and Srinivasan, M. S., 1983. *Neogene Planktonic Foraminifera: A Phylogenetic Atlas:* Stroudsburg, PA (Hutchinson Ross).

Kent, D. V., and Gradstein, F. M., 1985. A Cretaceous and Jurassic geochronology. *Geol. Soc. Am. Bull.,* 96:1419–1427.

Loeblich, A., and Tappan, H., 1987. *Foraminiferal Genera and Their Classification:* New York (Van Nostrand).

Manheim, F. T., and Sayles, F. L., 1974. Composition and origin of interstitial waters of marine sediments based on deep sea drill cores. *In* Goldberg, E. D. (Ed.), *The Sea* (Vol. 5): *Marine Chemistry:* New York (Wiley-Interscience), 527–568.

Martini, E., 1971. Standard Tertiary and Quaternary calcareous nannoplankton zonation. *In* Farinacci, A. (Ed.), *Proceedings of the Second International Conference on Planktonic Microfossils, Roma:* Rome (Ed. Technoscienza), 2:739–785.

Mayer, L. A., Courtney, R. C., and Moran, K., 1987. Ultrasonic measurements of marine sediment properties. *Proc. Oceanogr.,* 87 1:139.

Mazzullo, J. M., Meyer, A., and Kidd, R., 1988. New sediment classification scheme for the Ocean Drilling Program. *In* Mazzullo, J., and Graham, A. G., *Handbook for Shipboard Sedimentologists.* ODP Tech. Note, 8:45–67.

Norrish, K., and Hutton, J. T., 1969. An accurate X-ray spectrographic method for the analysis of a wide range of geological samples. *Geochim. Cosmochim. Acta,* 33:431–453.

Pezard, P. A., and Luthi, S. M., 1988. Borehole electrical images in the basement of the Cajon Pass Scientific Drillhole, California; fracture identification and tectonic implications. *Geophys. Res. Lett.,* 15: 1017–1020.

Pyle, M. R., 1984. Vane shear data on undrained residual strength. *J. Tech. Div., Am. Soc. Civ. Eng.,* 110:543–547.

Resig, J., 1981. Biogeography of benthic foraminifera on the northern Nazca Plate and adjacent continental margin. *Mem. Geol. Soc. Am.,* 154:619–666.

Riedel, W. R., and Sanfilippo, A., 1978. Stratigraphy and evolution of tropical Cenozoic radiolarians. *Micropaleontology,* 24:61–96.

Rio, D., Backman, J., and Raffi, I., in press. *Calcareous Nannofossil Biochronology and the Pliocene/Pleistocene Boundary:* Cambridge (Cambridge Univ. Press).

Rio, D., Fornaciari, E., and Raffi, I., 1990. Late Oligocene through early Pleistocene calcareous nannofossils from western equatorial Indian Ocean (Leg 115). *In* Duncan, R. A., Backman, J., Peterson, L. C., et al., *Proc. ODP, Sci. Results,* 115: College Station, TX (Ocean Drilling Program), 175–236.

Roth, P. H., and Thierstein, H. R., 1972. Calcareous nannoplankton: Leg 14 of the Deep Sea Drilling Project. *In* Hayes, D. E., Pimm, A. C., et al., *Init. Repts. DSDP,* 14: Washington (U.S. Govt. Printing Office), 421–485.

Sanfilippo, A., and Riedel, W. R., 1985. Cretaceous radiolaria. *In* Bolli, H. M., Saunders, J. B., and Perch-Nielsen, K. (Eds.), *Plankton Stratigraphy:* Cambridge (Cambridge Univ. Press), 573–630.

Sanfilippo, A., Westberg-Smith, M. J., and Riedel, W. R., 1985. Cenozoic radiolaria. *In* Bolli, H. M., Saunders, J. B., and Perch-Nielsen, K. (Eds.), *Plankton Stratigraphy:* Cambridge (Cambridge Univ. Press), 631–712.

Sato, T., Kameo, K., and Takayama, T., 1991. Coccolith biostratigraphy of the Arabian Sea and a new nannofossil zonal scheme for the Quaternary. *In* Prell, W. L., Niitsuma, N., et al., *Proc. ODP, Sci. Results,* 117: College Station, TX (Ocean Drilling Program).

Saunders, J. B., Bernoulli, D., Müller-Merz, E., Oberhänsli, H., Perch-Nielsen, K., Riedel, W. R., Sanfilippo, A., and Torrini, R., Jr., 1984. Stratigraphy of late middle Eocene to early Oligocene in the Bath Cliff section, Barbados, West Indies. *Micropaleontology,* 30: 390–425.

Schrader, H.-J., and Gersonde, R., 1978. Diatoms and silicoflagellates. *Utrecht Micropaleontol. Bull.,* 17:129–176.

Shipboard Scientific Party, 1988a. Introduction and explanatory notes. *In* Ruddiman, W., Sarnthein, M., et al., *Proc. ODP, Init. Repts.,* 108: College Station, TX (Ocean Drilling Program), 5–28.

________, 1988b. Introduction and explanatory notes. *In* Mascle, A., Moore, J. C., et al., *Proc. ODP, Init. Repts.,* 110: College Station, TX (Ocean Drilling Program), 5–25.

________, 1988c. Explanatory notes: Leg 112. *In* Suess, E., von Huene, R., et al., *Proc. ODP, Init. Repts.,* 112: College Station, TX (Ocean Drilling Program), 25–44.

________, 1989a. Explanatory notes. *In* Prell, W. L., Niitsuma, N., et al., *Proc. ODP, Init. Repts.,* 117: College Station, TX (Ocean Drilling Program), 11–33.

________, 1989b. Introduction and explanatory notes. *In* Robinson, P. T., Von Herzen, R., et al., *Proc. ODP, Init. Repts.,* 118: College Station, TX (Ocean Drilling Program), 3–24.

________, 1990a. Explanatory notes. *In* Gradstein, F. M., Ludden, J. N., et al., *Proc. ODP, Init. Repts.,* 123: College Station, TX (Ocean Drilling Program), 27–59.

________, 1990b. Explanatory notes. *In* Tamaki, K., Pisciotto, K., Allan, J., et al., *Proc. ODP, Init. Repts.,* 128: College Station, TX (Ocean Drilling Program), 35–60.

Sissingh, W., 1977. Biostratigraphy of Cretaceous calcareous nannoplankton. *Geol. Mijnbouw,* 56:37–65.

Sliter, W. V., 1989. Biostratigraphic zonation for Cretaceous planktonic foraminifers examined in thin section. *J. Foraminiferal Res.,* 19:1–19.

Stainforth, R. M., Lamb, J. L., Luterbacher, H. P., Beard, J. H., and Jeffords, R. M., 1975. Cenozoic planktonic foraminiferal zonation and characteristics of index forms. *Univ. Kans. Paleontol. Contrib. Art.,* 62:1–425.

Thierstein, H. R., 1976. Mesozoic calcareous nannoplankton biostratigraphy of marine sediments. *Mar. Micropaleontol.,* 1:325–362.

Thierstein, H. R., Geitzenauer, K. R., Molfino, B., and Shackleton, N. J., 1977. Global synchroneity of late Quaternary coccolith datum levels: validation by oxygen isotopes. *Geology,* 5:400–405.

Thomas, E., 1985. Late Eocene to Recent deep-sea benthic foraminifers from the central equatorial Pacific Ocean. *In* Mayer, L., Theyer, F., Thomas, E., et al., *Init. Repts. DSDP,* 85: Washington (U.S. Govt. Printing Office), 655–694.

van Morkhoven, F.P.C.M., Berggren, W. A., and Edwards, A. S., 1986. Cenozoic cosmopolitan deep-water benthic foraminifera. *Bull. Cent. Rech. Explor.-Prod. Elf-Aquitaine,* Mem. No. 11.

Vacquier, V., 1985. The measurement of thermal conductivity of solids with a transient linear heat source on the plane surface of a poorly conducting body. *Earth Planet. Sci. Lett.,* 74:275–279.

Von Herzen, R. P., and Maxwell, A. E., 1959. The measurement of thermal conductivity of deep-sea sediments by a needle probe method. *J. Geophys. Res.,* 65:1557–1563.

Wentworth, C. K., 1922. A scale of grade and class terms of clastic sediments. *J. Geol.,* 30:377–390.

Zijderveld, J.D.A., Zachariasses, J. W., Verhallen, P.J.J.M., and Hilgen, F. J., 1986. The age of the Miocene-Pliocene boundary. *Newsl. Stratigr.,* 16:169–181.

Zoback, M. D., Zoback, M. L., Mount, V. S., Suppe, J., Eaton, J. P., Healy, J. H., Oppenheimer, D., Reasenberg, P., Jones, L., Raleigh, C. B., Wong, I. G., Scotti, O., and Wentworth, C., 1988. New evidence on the state of stress of the San Andreas Fault. *Science,* 238: 1105–1111.

Ms 130A-102